



## **H<sub>2</sub>-dominated Atmosphere as an Indicator of Second-generation Rocky White Dwarf Exoplanets**

**Lin, Zifan; Seager, Sara; Ranjan, Sukrit; Kozakis, Thea; Kaltenegger, Lisa**

*Published in:*  
The Astrophysical Journal Letters

*Link to article, DOI:*  
[10.3847/2041-8213/ac4788](https://doi.org/10.3847/2041-8213/ac4788)

*Publication date:*  
2022

*Document Version*  
Publisher's PDF, also known as Version of record

[Link back to DTU Orbit](#)

*Citation (APA):*  
Lin, Z., Seager, S., Ranjan, S., Kozakis, T., & Kaltenegger, L. (2022). H<sub>2</sub>-dominated Atmosphere as an Indicator of Second-generation Rocky White Dwarf Exoplanets. *The Astrophysical Journal Letters*, 925(1), Article L10. <https://doi.org/10.3847/2041-8213/ac4788>

---

### **General rights**

Copyright and moral rights for the publications made accessible in the public portal are retained by the authors and/or other copyright owners and it is a condition of accessing publications that users recognise and abide by the legal requirements associated with these rights.

- Users may download and print one copy of any publication from the public portal for the purpose of private study or research.
- You may not further distribute the material or use it for any profit-making activity or commercial gain
- You may freely distribute the URL identifying the publication in the public portal

If you believe that this document breaches copyright please contact us providing details, and we will remove access to the work immediately and investigate your claim.



# H<sub>2</sub>-dominated Atmosphere as an Indicator of Second-generation Rocky White Dwarf Exoplanets

Zifan Lin<sup>1</sup> , Sara Seager<sup>2,3</sup>, Sukrit Ranjan<sup>1,4,5,6</sup> , Thea Kozakis<sup>7</sup> , and Lisa Kaltenegger<sup>8</sup> <sup>1</sup> Department of Earth, Atmospheric, and Planetary Sciences, Massachusetts Institute of Technology, 77 Massachusetts Avenue, Cambridge, MA 02139, USA<sup>2</sup> Department of Physics, Massachusetts Institute of Technology, 77 Massachusetts Avenue, Cambridge, MA 02139, USA<sup>3</sup> Department of Aeronautics and Astronautics, Massachusetts Institute of Technology, 77 Massachusetts Avenue, Cambridge, MA 02139, USA<sup>4</sup> Northwestern University, Center for Interdisciplinary Exploration and Research in Astrophysics, Evanston, 60201, USA<sup>5</sup> Northwestern University, Department of Astronomy & Astrophysics, Evanston, 60201, USA<sup>6</sup> Blue Marble Space Institute of Science, Seattle, 98154, USA<sup>7</sup> DTU Space, National Space Institute, Technical University of Denmark, Elektrovej 328, DK-2800 Kgs. Lyngby, Denmark<sup>8</sup> Carl Sagan Institute and Department of Astronomy, Cornell University, Ithaca, NY 14853, USA

Received 2021 October 20; revised 2021 December 22; accepted 2021 December 30; published 2022 January 26

## Abstract

Following the discovery of the first exoplanet candidate transiting a white dwarf (WD), a “white dwarf opportunity” for characterizing the atmospheres of terrestrial exoplanets around WDs is emerging. Large planet-to-star size ratios and hence large transit depths make transiting WD exoplanets favorable targets for transmission spectroscopy; conclusive detection of spectral features on an Earth-like planet transiting a close-by WD can be achieved within a medium James Webb Space Telescope program. Despite the apparently promising opportunity, however, the post-main sequence evolutionary history of a first-generation WD exoplanet has never been incorporated in atmospheric modeling. Furthermore, second-generation planets formed in WD debris disks have never been studied from a photochemical perspective. We demonstrate that transmission spectroscopy can identify a second-generation rocky WD exoplanet with a thick ( $\sim 1$  bar) H<sub>2</sub>-dominated atmosphere. In addition, we can infer outgassing activities of a WD exoplanet based on its transmission spectra and test photochemical runaway by studying CH<sub>4</sub> buildup.

*Unified Astronomy Thesaurus concepts:* [Exoplanet atmospheres \(487\)](#); [Exoplanets \(498\)](#); [Exoplanet evolution \(491\)](#); [White dwarf stars \(1799\)](#)

## 1. Introduction

An exciting opportunity for characterizing the atmospheres of terrestrial exoplanets transiting white dwarfs (WDs) is emerging. The first planet candidate transiting a WD was discovered in the WD 1856+534 system (Vanderburg et al. 2020), followed by a recent microlensing detection of a gas giant in a Jupiter-like orbit around a WD (Blackman et al. 2021). Kaltenegger et al. (2020) explored the possibility of observing transiting Earth-like WD planets with James Webb Space Telescope (JWST) and described a “white dwarf opportunity” of detecting biosignature gases on such planets. Due to their large planet-to-star radius ratio, WD exoplanets have much larger transit depths compared to planets around main-sequence (MS) hosts, making them favorable targets for transmission spectroscopy (e.g., Agol 2011; Loeb & Maoz 2013). For a hypothetical Earth-sized planet with Earth-like atmosphere transiting WD 1856+534, JWST can detect H<sub>2</sub>O and CO<sub>2</sub> with just a few transits and detect biosignature gases such as the O<sub>3</sub> + CH<sub>4</sub> pair in 25 transits (Kaltenegger et al. 2020). For comparison, JWST would struggle to detect the O<sub>3</sub> + CH<sub>4</sub> biosignature pair on a terrestrial planet orbiting an M dwarf such as TRAPPIST-1e even with 100 transits (e.g., Lin et al. 2021).

There have been some pioneering works on photochemical modeling of WD exoplanets, but those works are naturally

limited in the parameter space explored. Kozakis et al. (2018, 2020) modeled Earth-mass planets orbiting WDs with N<sub>2</sub>-dominated atmospheres, modern Earth-like O<sub>2</sub> and CO<sub>2</sub> concentrations, and modern-Earth-like outgassing rates for key spectral species including CH<sub>4</sub> and N<sub>2</sub>O. Kaltenegger et al. (2020) analyzed the detectability of spectral signatures by JWST for Earth-like rocky WD exoplanets, based on the models developed by Kozakis et al. (2018, 2020).

While Earth-like composition is an important possibility to include, the atmosphere of an Earth-mass rocky planet may span different oxidation states, from reducing to oxidizing. Therefore, here we attempt to expand our knowledge of putative Earth-mass exoplanets in WD systems by exploring the vast uncharted parameter space from an atmospheric modeling perspective. We follow the “exoplanet benchmark cases” outlined by Hu et al. (2012) and consider three types of atmospheric compositions, including reducing (H<sub>2</sub>-dominated), weakly oxidizing (N<sub>2</sub>-dominated), and oxidizing (CO<sub>2</sub>-dominated) atmospheres. Furthermore, the evolutionary history of a first-generation WD exoplanet is distinct from an MS planet like Earth, and the formation origin of a second-generation WD exoplanet is also different from Earth’s. Affected by their origin and evolution, WD exoplanets can have atmospheric compositions and surface emissions distinct from Earth. Therefore, it is necessary to incorporate the unique evolutionary history of WD exoplanets when modeling their atmospheres.

Due to the large scale height of H<sub>2</sub>-dominated atmospheres, H<sub>2</sub> atmospheres on Earth-mass planets are much easier for JWST to detect and characterize compared to high mean molecular weight (MMW) atmospheres, so we place special emphasis on H<sub>2</sub>-dominated atmospheres. In addition, for H<sub>2</sub>



Original content from this work may be used under the terms of the [Creative Commons Attribution 4.0 licence](#). Any further distribution of this work must maintain attribution to the author(s) and the title of the work, journal citation and DOI.

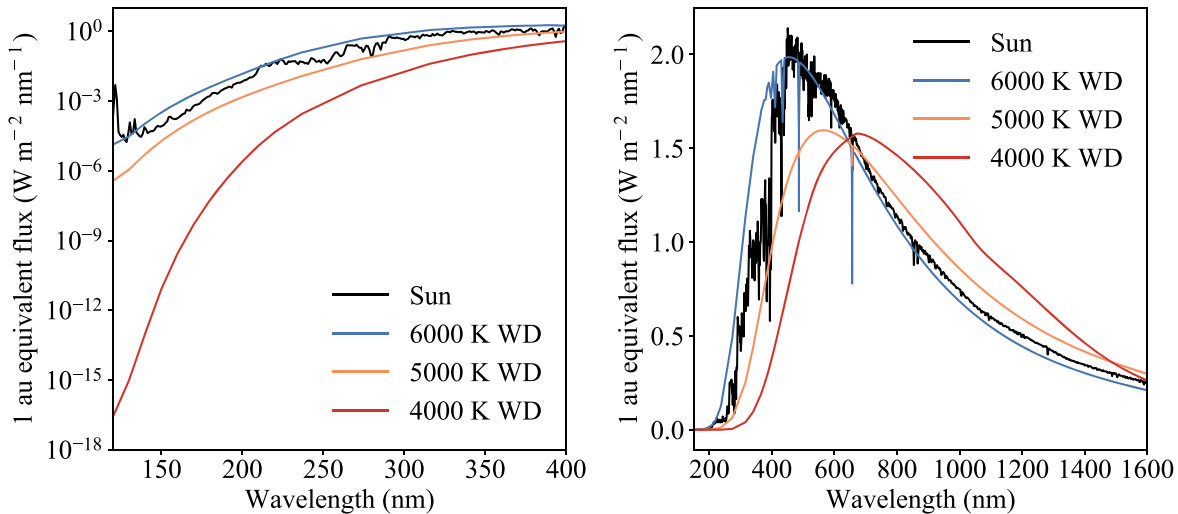


**Figure 1.** Irradiation received at the top of atmosphere for planets orbiting WDs at 1 au equivalent distance. In our models, 1 au equivalent distance means the WD planets receive the same integrated flux as modern Earth around the Sun. The stellar spectra are shown for (left) UV wavelengths and (right) 150–1600 nm. The solar spectrum is shown as black solid lines. The spectra for WDs with effective temperatures of 6000 K, 5000 K, and 4000 K are shown as blue, orange, and red solid lines, respectively. The UV spectra (left) show that the 6000 K WD has similar extreme-UV (EUV; <124 nm) intensity as the Sun, while the 5000 K WD and 4000 K WD have  $\sim 10^3$  and  $>10^{10}$  times lower EUV intensity than the Sun, respectively (Saumon et al. 2014). The overall spectra (right) show that WD spectra are almost perfect blackbodies, while the solar spectrum shows abundant absorption lines, which explains the difficulty of constraining masses of WD exoplanets using the radial velocity method (Vanderburg et al. 2020).

atmospheres, a low ultraviolet (UV) radiation environment can facilitate biosignature gas accumulation (e.g., Seager et al. 2013), and we discuss the photochemical implications of  $\text{H}_2$  atmospheres around cool WDs, which have extremely low UV.

In what follows, we introduce our input WD stellar spectra and models in Section 2. We present our main results for  $\text{H}_2$ -dominated atmospheres in Section 3 and main results for  $\text{N}_2$ - and  $\text{CO}_2$ -dominated atmospheres in Section 4. Section 5 contains the discussion, and we summarize our conclusions in Section 6.

## 2. Methods

### 2.1. Stellar Model

Following Kozakis et al. (2018, 2020), we use cool WD spectral models calculated by Saumon et al. (2014) for WD temperatures of 6000, 5000, and 4000 K to represent WD cooling throughout time. These models assume an average WD mass of  $0.6 M_\odot$  (Kepler et al. 2016) with pure hydrogen atmospheres and surface gravities of  $\log g = 8.0$ . Due to the high surface gravity, these WD atmospheres are highly differentiated and only display Balmer absorption lines for temperatures  $\gtrsim 5000$  K, with hydrogen becoming neutral at lower temperatures (as seen in Figure 1). For further discussions on spectral modeling methods for cool WD atmospheres, see, e.g., Saumon et al. (2014), Kozakis et al. (2018), and references therein.

### 2.2. Photochemistry Model

We use a 1D photochemistry model that was validated by simulating the atmospheric compositions of modern Earth and Mars (Hu et al. 2012), with  $\text{CO}_2$  and  $\text{H}_2\text{O}$  cross sections updated by Ranjan et al. (2020). The photochemistry model was manually coupled with an analytical atmospheric temperature model formulated by Guillot (2010) implemented as a part of the petitRADTRANS radiative transfer package

(Mollière et al. 2019). Converged atmospheric chemical profiles are shown in Figure 2.

We assume three types of anoxic atmospheres following the exoplanet benchmark scenarios presented by Hu et al. (2012). The benchmark scenarios include a reducing (90%  $\text{H}_2$ , 10%  $\text{N}_2$ ), a weakly oxidizing (>99%  $\text{N}_2$ ), and an oxidizing (90%  $\text{CO}_2$ , 10%  $\text{N}_2$ ) atmosphere. For each atmospheric scenario, we assume two sets of outgassing rates for  $\text{CO}_2$ ,  $\text{H}_2$ ,  $\text{SO}_2$ ,  $\text{CH}_4$ , and  $\text{H}_2\text{S}$ , one corresponding to modern Earth-like volcanic emission rates, and the other corresponding to a less geologically active planet outgassing at 1000 times lower rates.

We assume Earth-like parameters— $1 M_\oplus$  mass,  $1 R_\oplus$  radius, and 1 bar surface pressure—for all planets modeled. For the  $\text{N}_2$ -dominated atmospheric models, we assume the planet is located at the 1 au equivalent distance, which means that the planet receives the same integrated flux as Earth’s irradiation on top of its atmosphere. Due to an enhanced greenhouse effect, planets with  $\text{CO}_2$ - and  $\text{H}_2$ -dominated atmospheres are placed at 1.3 au and 1.6 au equivalent distance to maintain similar surface temperature conditions. For more details of the photochemistry model, refer to Appendix A.1.

### 2.3. Transmission Spectra Model

We use a publicly available Python package petitRADTRANS (Mollière et al. 2019) to calculate the transmission spectra for all of our planet models, using our photochemistry code results as inputs. We apply the low-resolution correlated-k method to generate spectra with  $\lambda/\Delta\lambda = 1000$ . We generate 100 atmospheric layers with pressures distributed equidistantly in log space, starting from the surface (1 bar) to the top of atmosphere ( $\sim 10^{-7}$  bar).

Cloud layers mute spectral signatures by blocking molecules below from the view of an observer (see, e.g., Komacek et al. 2020; Suissa et al. 2020 for recent 3D explorations). In addition, atmospheric refraction may prevent transmission spectroscopy from accessing the lower atmosphere by bending light rays away from a distant observer (e.g., Bétrémieux &

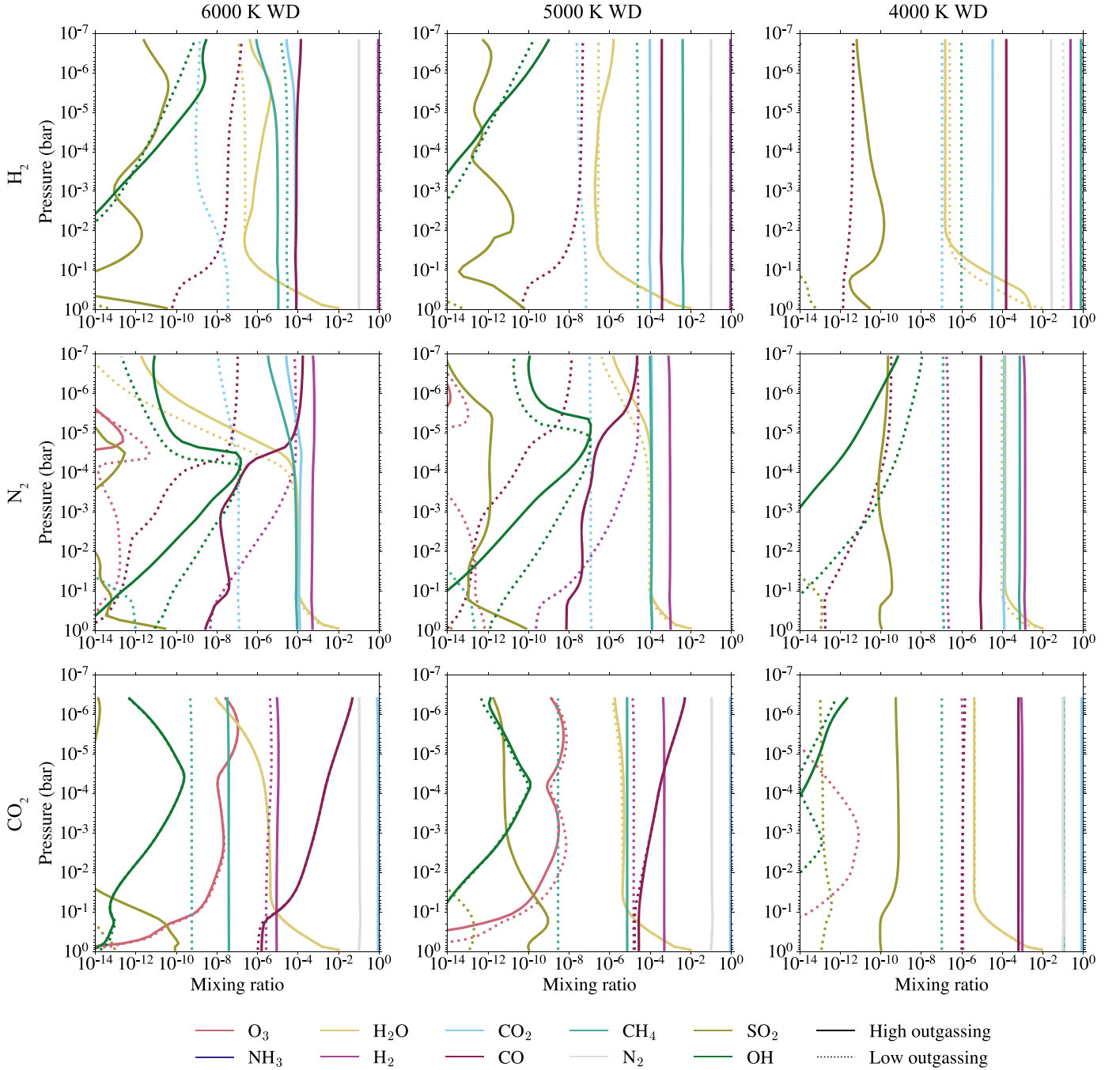


**Figure 2.** Chemical mixing ratios for our model planets. We compare high outgassing rates (solid lines) with low outgassing rates (dotted lines).  $\text{H}_2$ -,  $\text{N}_2$ -, and  $\text{CO}_2$ -dominated atmospheres are shown in the top, middle, and bottom rows, respectively. The left, middle, and right columns show WDs with effective temperatures of 6000 K, 5000 K, and 4000 K, respectively. Mixing ratios of volcanically produced gases, such as  $\text{CH}_4$ ,  $\text{CO}_2$ , and  $\text{SO}_2$ , are generally higher in the high outgassing models. Mixing ratios of photochemically destroyed gases such as  $\text{CH}_4$  are generally higher in the cooler WD models, due to less UV irradiation.

Kaltenegger 2014; Robinson et al. 2017). Effects of clouds and refraction are both accounted for in our transmission spectra model. For more details of the transmission spectra model, refer to Appendix A.2.

#### 2.4. Simulated JWST Observations

We simulate JWST observations of our model rocky WD exoplanets with the NIRSpec Prism instrument using PandExo (Batalha et al. 2017). For all simulations, we limit saturation

level to 80% and do not bin the output spectra. For stellar input parameters, we use the physical properties of WD 1856+534 reported by Vanderburg et al. (2020):  $J$ -band magnitude = 15.677 and stellar radius =  $0.0131 R_\odot$ . For planet parameters, we use the transmission spectra generated by petitRADTRANS as the input spectra, assuming a  $1 R_\oplus$  planet radius and a 2 minute transit duration, which is the transit duration of a planet in the habitable zone (HZ) of WD 1856+534 (e.g., Kaltenegger et al. 2020). All other observational parameters are optimized by PandExo under the default settings. We simulated a range of

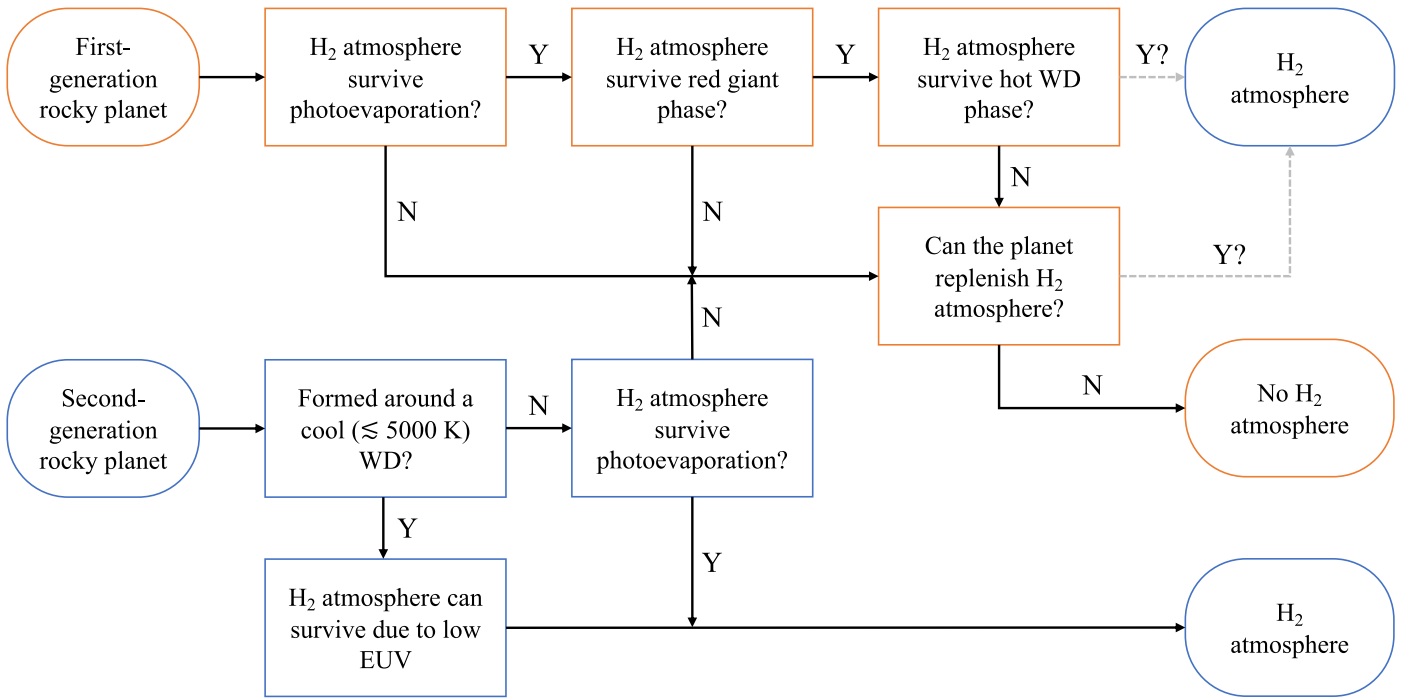


**Figure 3.** Flowchart showing evolution of  $\text{H}_2$  atmospheres on first- and second-generation rocky WD exoplanets. Plausible evolutionary pathways are shown as solid black arrows, while improbable pathways are shown as dashed gray arrows. The main takeaway from this flowchart is that retention of  $\text{H}_2$  atmospheres on first-generation Earth-mass rocky planets requires a sequence of unlikely coincidences, while second-generation rocky WD planets have a viable pathway to produce and maintain an  $\text{H}_2$ -dominated atmosphere.

JWST campaign sizes: one transit, five transits, 10 transits, and 25 transits, which correspond to 2, 10, 20, and 50 minutes of total in-transit integration time, respectively.

### 3. Results

Here we demonstrate in Section 3.1 that a thick ( $\sim 1$  bar)  $\text{H}_2$ -dominated atmosphere on a rocky WD exoplanet is an indicator of a second-generation Earth-mass planet. We show that such  $\text{H}_2$  atmospheres are easily detectable by JWST and discuss the implications of our simulated transmission spectra in Sections 3.2–3.4. Detectability of key spectral features by JWST is summarized in Appendix C.

#### 3.1. $\text{H}_2$ -dominated Atmospheres as Indicators of Second-generation Planets

Here we we qualitatively discuss the evolution of an  $\text{H}_2$ -dominated atmosphere. Quantitative results supporting the qualitatively analysis are shown in Appendix B.

##### 3.1.1. Evolution of $\text{H}_2$ -dominated Atmospheres on WD Exoplanets

We begin our evolutionary analysis by considering an Earth-mass planet formed around the young MS progenitor (top row, Figure 3). Primary  $\text{H}_2$  envelopes of an Earth-mass rocky planet may experience photoevaporation due to the excessive extreme-UV (EUV) radiation produced by young stars (e.g., Owen & Wu 2013; Lopez & Fortney 2013). A terrestrial planet either loses its hydrogen atmosphere entirely and remains a barren core with a radius distribution that peaks at  $\sim 1.3 R_\oplus$ , or retains a very thick envelope that doubles the core’s radius, creating an “evaporation valley” in the radius distribution of known exoplanets (e.g., Owen &

Wu 2017). A more recent work argues that  $\sim 2 M_\oplus$  rocky planets with  $\text{H}_2$  envelopes may have already been discovered, and even lower-mass planets with voluminous  $\text{H}_2$  atmospheres possibly exist (Owen et al. 2020). Hence, first-generation  $\text{H}_2$ -rich rocky planets cannot be ruled out on the basis of photoevaporation.

Even if the  $\text{H}_2$  envelope on an Earth-mass exoplanet survives the MS phase, it is likely to be lost in the post-MS evolution. The red-giant phase and the hot WD phase can both threaten  $\text{H}_2$  atmospheres. As a red giant loses its gaseous envelope, stellar winds due to mass loss can erode atmospheres (e.g., Ramirez & Kaltenegger 2016; Kozakis & Kaltenegger 2019). Outward migration is therefore necessary for atmospheric retention. Such orbital expansion can be triggered by red-giant mass loss (e.g., Schröder & Smith 2008).

A hydrogen-dominated atmosphere on an Earth-mass planet is very unlikely to survive the hot WD phase, even if it fortuitously survived both the MS phase and the red-giant phase. Young WDs initially have very high effective temperatures ( $T_{\text{eff}}$ ) and intense EUV radiation. When a solar-mass star turns into a WD, it will start with  $T_{\text{eff}} \gtrsim 100,000$  K and then experience quasi-exponential radiative cooling to  $\sim 30,000$  K in a time span of approximately 10 Myr (Fontaine et al. 2001). High  $T_{\text{eff}}$  results in EUV intensity. An exoplanet orbiting a hot WD will be bombarded by excessive EUV radiation up to a million times higher than modern solar levels, resulting in rapid atmospheric mass loss even if the planet migrates to an orbital distance of 50–100 au (Schreiber et al. 2019). Volcanic  $\text{H}_2$  emission cannot compensate such loss (Figure 4). We therefore conclude that the EUV radiation from hot WDs will cause total erosion of hydrogen atmospheres. In Appendix B we quantitatively prove this conclusion.

Given that the survival of a primarily hydrogen atmosphere on an Earth-mass first-generation WD exoplanet is highly

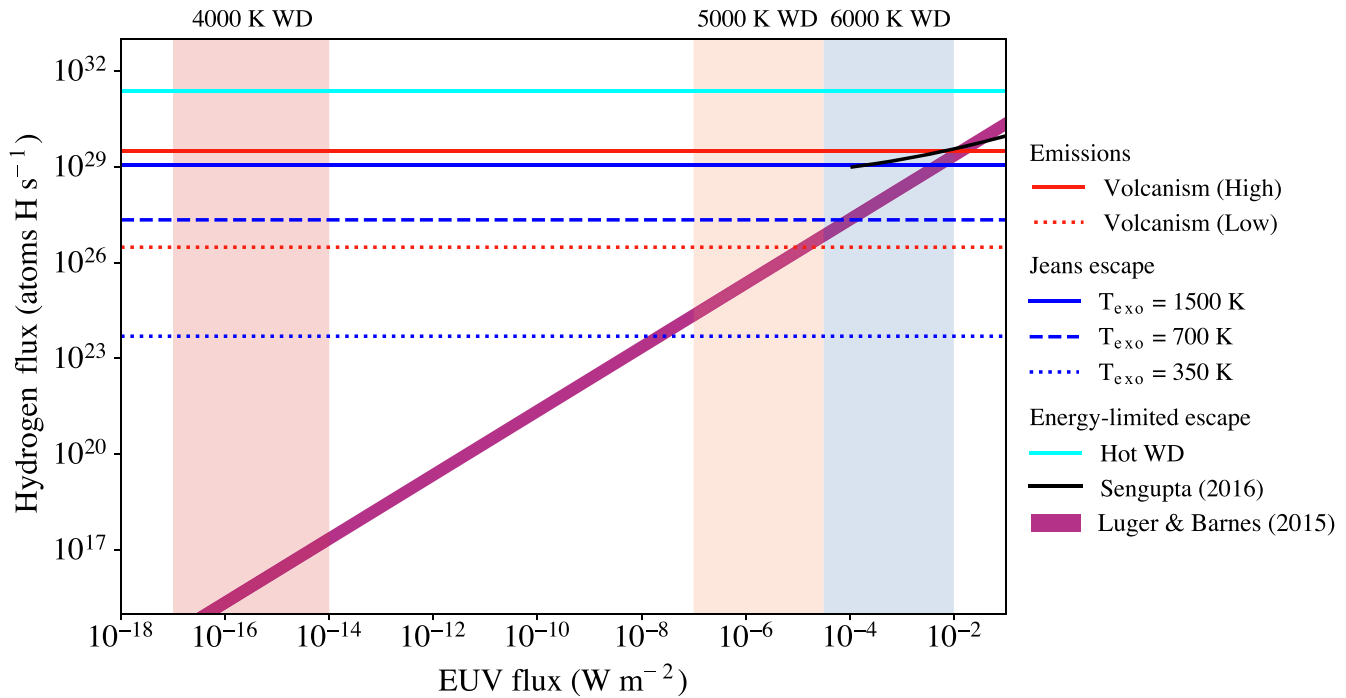


**Figure 4.** Volcanic emission rates and escape rates of hydrogen in atmospheres of  $1 M_{\oplus}$  rocky WD exoplanets. The energy-limited escape rates (purple and black solid lines) are functions of EUV flux received by the planet, while all other lines are independent of flux or assume a fixed flux. The red solid line and the red dotted line represent high and low volcanic emission rates of  $H_2$ , respectively. The high emission rate is 20 times higher than the modern Earth  $H_2$  emission rate and 1000 times higher than the low emission rate. The blue solid line, blue dashed line, and blue dotted line demarcate the Jeans escape rates assuming exobase temperatures of 1500 K (roughly the maximum exospheric temperature on Earth), 700 K (roughly the minimum exospheric temperature on Earth), and 350 K (exobase temperature on Mars), respectively. The cyan solid line is the energy-limited escape rate of a planet orbiting a 40,000 K hot WD at a distance of  $\sim 50\text{--}80$  au (Schreiber et al. 2019). The black solid line is the energy-limited escape rate calculated based on the Watson et al. (1981) and Sengupta (2016) formulas, which are only solvable for a certain range. The purple solid line shows a range of energy-limited escape rates assuming different  $\epsilon_{\text{EUV}}$  and  $R_{\text{EUV}}$  for a sensitivity test (Luger & Barnes 2015). The approximate ranges of EUV radiation received by planets at 1 au equivalent distance orbiting 4000 K, 5000 K, and 6000 K WDs are shown as red, orange, and blue rectangles, respectively. Implications of this figure are: (i) energy-limited escape driven by excessive EUV of hot WDs will erode  $H_2$  atmospheres even if the planets have high  $H_2$  emission rate, and (ii) maintaining  $H_2$ -dominated atmospheres is possible for planets with high outgassing rates orbiting all three types of WDs, and is possible for planets with low outgassing rates orbiting cool ( $\lesssim 5000$  K) WDs, assuming suitable exobase temperatures. For numerical details, see Appendix B.

unlikely, replenishing an  $H_2$ -dominated atmosphere via outgassing remains as the only possibility. We will show in Section 3.1.2 that replenishing hydrogen by outgassing is unlikely for a first-generation planet.

We now shift the focus to second-generation Earth-mass planets and show that planets formed in the debris disks of WDs can possibly maintain a detectable  $H_2$ -dominated atmosphere (bottom row, Figure 3). Protoplanets can form in tight orbits around WDs via coagulation of viscously spreading disk materials, and then the protoplanets can further accrete disk material to form major planets just outside the Roche limit of the host WD. If a super-Earth is tidally destroyed, this formation mechanism can potentially recycle materials, including volatile materials such as water, from the disrupted planet to form an Earth-mass planet (Bear & Soker 2015; van Lieshout et al. 2018).

Second-generation planets can form at any time during a WD’s lifetime. Formation of second-generation WD planets is possible whenever planetary materials are delivered into a WD’s Roche limit and be tidally disrupted (Bear & Soker 2015; van Lieshout et al. 2018). Such delivery can occur at any time during a WD’s lifetime, because WD pollutants have been detected on WDs across temperature ranges. The coolest polluted WD has an effective temperature of  $\sim 4000$  K (Coutu et al. 2019), evidencing that some of the oldest known WDs are actively accreting materials, so second-generation planet formation can occur around cool WDs.

Second-generation planets formed around  $>6000$  K WDs are also vulnerable to photoevaporation because of their modern Sun-like UV radiation (Figure 1).

A hydrogen atmosphere can survive, however, if the planet forms around a cool ( $\lesssim 5000$  K) WD. EUV intensity of a 5000 K WD is  $\sim 100\text{--}1000$  times less than that of the modern Sun, while a 4000 K WD emits  $\gtrsim 10^{10}$  times less EUV radiation than the modern Sun (Figure 1). Both types of dominant neutral atmospheric escape mechanisms—Jeans escape (e.g., Hunten 1973) and hydrodynamic escape (Watson et al. 1981; Luger & Barnes 2015; Sengupta 2016)—are powered by EUV radiation. We will show quantitatively in Appendix B that given the low EUV intensity of  $\lesssim 5000$  K WDs, high to moderate volcanic hydrogen emission rates are sufficient to sustain an  $H_2$ -dominate atmosphere (Figure 4).

In summary, the most viable path to a roughly 1 bar  $H_2$ -dominated atmosphere on an Earth-mass WD exoplanet is provided by second-generation planets formed around cool WDs (Figure 3). Survival of  $H_2$  atmospheres on first-generation rocky WD exoplanets requires a sequence of improbable coincidence.

### 3.1.2. First-generation Planets Cannot Replenish $H_2$ Atmosphere via Outgassing

Once the  $H_2$ -dominated atmosphere on a first-generation rocky planet is lost, replenishing a secondary  $H_2$  atmosphere via outgassing is unlikely. Replenishing a reduced hydrogen

**Table 1**  
 $\sigma$  Significance of Ruling Out a Flat Line Based on Transmission Spectra

	N <sub>2</sub> Atmospheres			CO <sub>2</sub> Atmospheres			H <sub>2</sub> Atmospheres		
	4000 K	5000 K	6000 K	4000 K	5000 K	6000 K	4000 K	5000 K	6000 K
<i>High Outgassing</i>									
1 NIRSpec Prism transit	2.7	5.2	6.6	5.1	4.7	2.3	>10	>10	>10
5 NIRSpec Prism transits	>10	6.8	7.5	7.5	7.8	7.4	>10	>10	>10
<i>Low outgassing</i>									
	N <sub>2</sub> Atmospheres			CO <sub>2</sub> Atmospheres			H <sub>2</sub> Atmospheres		
	4000 K	5000 K	6000 K	4000 K	5000 K	6000 K	4000 K	5000 K	6000 K
1 NIRSpec Prism transit	3.4	3.7	3.6	4.3	3.7	4.4	>10	>10	>10
5 NIRSpec Prism transits	6.5	2.8	6.6	4.2	7.1	6.6	>10	>10	>10

atmosphere requires reducing volcanic emissions, neglecting other sources such as biogenic emission. Reduced volcanic emissions require reduced mantles. The dominant form of hydrogen outgassing on a planet with an oxidized mantle, such as present-day Earth, is H<sub>2</sub>O (Holland 1984). Molecular hydrogen is the dominant form of hydrogen emission only when the planet’s mantle is highly reduced (Ramirez et al. 2014; Ortenzi et al. 2020).

However, first-generation Earth-mass WD exoplanets are generally expected to have oxidized mantles because of mantle self-oxidation. The mantle of a  $\sim 1 M_{\oplus}$  rocky planet starts reduced, but becomes more oxidized over time due to gradual or stepwise self-oxidation (Scaillet & Gaillard 2011). Such self-oxidation is thought to be a natural consequence of the size of Earth-mass rocky planets (Wood et al. 2006). Similarity in bulk composition between WD exoplanets and the Earth is inferred by WD pollution (e.g., Farihi et al. 2016; Doyle et al. 2019). Due to compositional resemblance, we expect Earth-mass first-generation WD planets would undergo the same self-oxidation process.

Mantle self-oxidation of Earth-mass rocky planets occurs within  $\sim 100$  Myr (Trail et al. 2011), which is much shorter compared to the age of first-generation WD exoplanets. The age of a first-generation WD exoplanet is the sum of an MS progenitor lifetime and a WD cooling time, which are both on the order of gigayears. Therefore, first-generation rocky WD planets do not have the right conditions to outgas hydrogen in the form of H<sub>2</sub>.

### 3.2. Transmission Spectra Can Differentiate between First- and Second-generation Planets

We have demonstrated that theoretically, the presence of H<sub>2</sub>-dominated atmospheres on Earth-mass WD exoplanets indicates second-generation planets. Observationally, JWST can potentially differentiate between first- and second-generation Earth-mass planets using H<sub>2</sub> atmospheres using only one NIRSpec Prism transit, assuming a  $1 R_{\oplus}$  planet transiting WD 1856+534.

An atmosphere is detectable if a null assumption (flat spectrum) can be ruled out conclusively. For each simulated NIRSpec Prism transmission observation, we find the best-fit horizontal line representing a flat spectrum and determine the  $\sigma$  significance of ruling out this flat line fit using a  $\chi^2$  analysis. Results are summarized in Table 1, and model transmission spectra overplotted with simulated observation data are shown

in Figure 5. Due to the large scale height of hydrogen atmospheres, one transit is sufficient to rule out a flat spectrum for all H<sub>2</sub>-dominated atmospheric models at  $>10\sigma$ .

High-altitude clouds or hazes layers can hide the atmosphere below, hence decreasing the detectability of the atmosphere. Our models assume an opaque global cloud layer at 0.47 bar ( $\approx 35$  km in H<sub>2</sub>-dominated atmospheres). Organic haze formation in atmospheres on rocky Earth-like exoplanets is studied (e.g., Arney et al. 2016, 2017, 2018) but not included in our atmospheric models, and will be discussed in Section 5.4.

### 3.3. Transmission Spectra Can Infer Outgassing Activities

Rocky WD exoplanets can have drastically different outgassing rates depending on their tectonic states. An Earth-mass rocky planet can possibly have three tectonic states: (i) active lid, where lithosphere strength is overwhelmed by convective stresses, and surface materials can be recycled into the mantle, (ii) stagnant lid, where the lithosphere is too rigid to be deformed and recycled into the mantle, and (iii) an episodic regime characterized by occasional lithosphere overturn (see, e.g., Lenardic et al. 2016 and references therein).

Conceptually, planets with Earth-like active plate tectonics can recycle atmospheric and oceanic volatiles back into the mantle to sustain continuous outgassing over long timescales (e.g., Kasting & Catling 2003), while stagnant lid planets cannot. Indeed, some have argued that Earth-mass stagnant lid planets would deplete mantle volatiles rapidly, and the outgassing rates would drop to negligible levels within  $\sim 1$ – $2$  Gyr (e.g., Foley & Smye 2018; Dorn et al. 2018). Therefore, differentiating between active lid and stagnant lid regimes on rocky WD exoplanets is ostensibly possible, if we can differentiate between the different outgassing scenarios with transmission spectroscopy.

However, the topic of rocky planet tectonics remains hotly debated, and the possibility of inferring tectonic activities from outgassing rates is challenged by several uncertainties. One major uncertainty is that rocky planets can alternate between multiple tectonic states over gigayear timescales (Weller et al. 2015), so we are agnostic about a planet’s tectonic history given only a snapshot of its present-day outgassing rates. In addition, even for the best-studied rocky planet—Earth—the onset and end of plate tectonics are highly uncertain (see, e.g., Rey et al. 2014; Weller et al. 2015 and references therein).

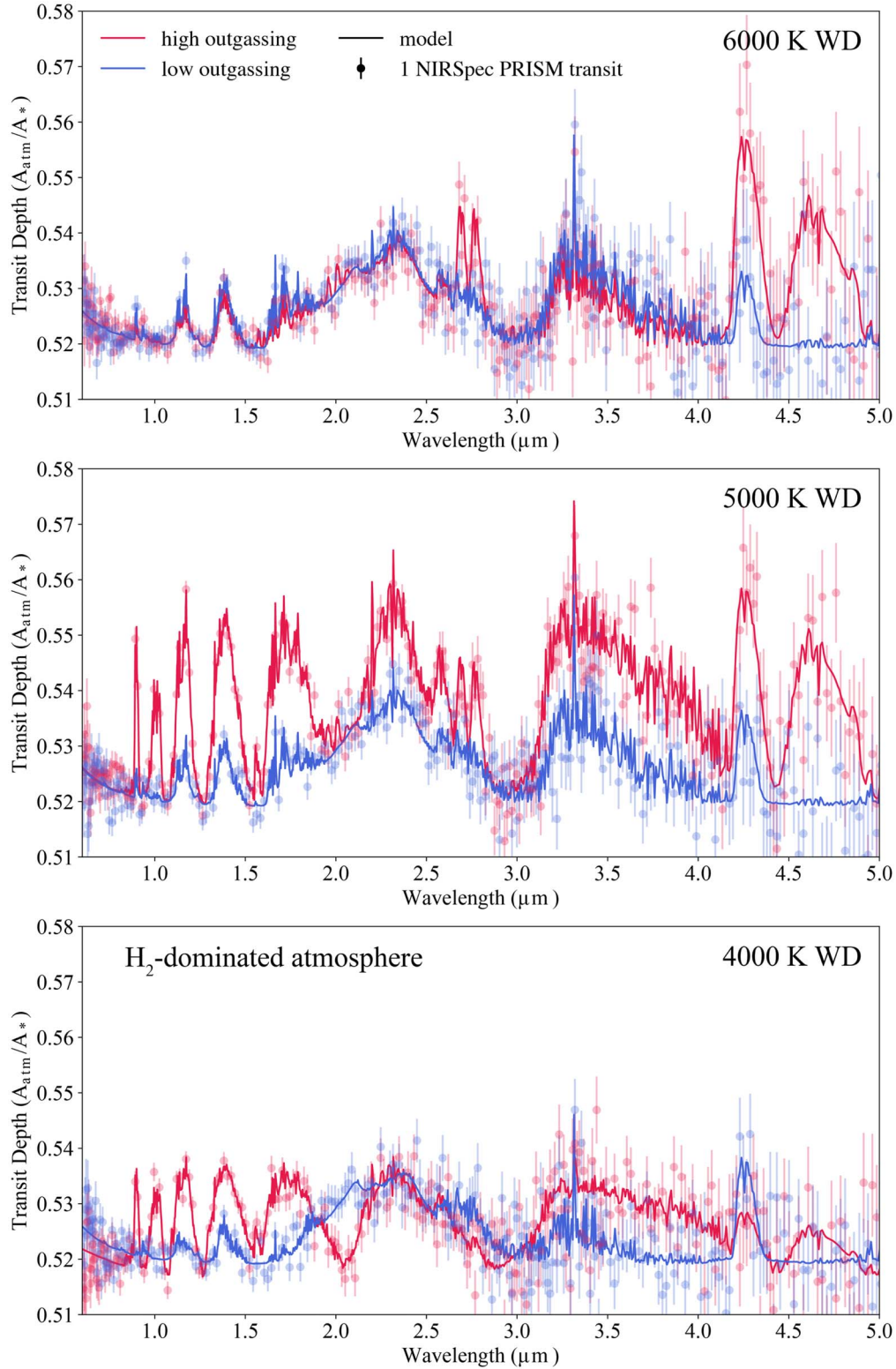


**Figure 5.** Transmission spectra models and simulated JWST transit observations for  $\text{H}_2$ -dominated atmospheres, assuming a  $1 R_{\oplus}$  planet transiting WD 1856+534. We compare high outgassing rate models (red solid lines) with low outgassing rate models (blue solid lines) and show simulated JWST data points with their  $1\sigma$  error bars. We assume one NIRSpec Prism transit for the  $\text{H}_2$ -dominated atmospheric models. In the  $\text{H}_2$ -dominated atmospheres, spectral signatures have high detectability, and differentiating between high and low outgassing scenarios is achievable with one transit.

Due to the uncertainties of rocky planet tectonic states, we do not intend to infer the tectonic activities or evolutionary history of rocky WD exoplanets from their atmospheres. Instead, we focus on the capability of transmission spectra to

differentiate between high and low outgassing scenarios, and leave the linkage between outgassing rates and tectonic states for future investigation. Here we consider planets with a thick ( $\sim 1$  bar) atmosphere and two outgassing rates: a high

**Table 2**  
Column-integrated CH<sub>4</sub> Mixing Ratios in Photochemistry Models

	H <sub>2</sub> Atmospheres		CO <sub>2</sub> Atmospheres		N <sub>2</sub> Atmospheres	
	High Outgassing	Low Outgassing	High Outgassing	Low Outgassing	High Outgassing	Low Outgassing
4000 K	0.73	$9.5 \times 10^{-7}$	0.1	$1.0 \times 10^{-7}$	$7.1 \times 10^{-4}$	$1.2 \times 10^{-7}$
5000 K	$4.2 \times 10^{-3}$	$2.4 \times 10^{-5}$	$7.2 \times 10^{-6}$	$2.8 \times 10^{-9}$	$1.2 \times 10^{-4}$	$1.7 \times 10^{-13}$
6000 K	$1.0 \times 10^{-5}$	$3.0 \times 10^{-5}$	$3.8 \times 10^{-8}$	$5.7 \times 10^{-10}$	$8.5 \times 10^{-5}$	$7.4 \times 10^{-13}$

outgassing rate corresponding to modern Earth-like volcanic emission rates (following Hu et al. 2012), and a low outgassing rate that is reduced by a factor of 1000.

Transmission spectra can differentiate between our high and low outgassing scenarios assuming H<sub>2</sub>-dominated atmospheres. The two outgassing scenarios can be differentiated because strong spectral absorbers such as CH<sub>4</sub> and CO<sub>2</sub> reach a higher equilibrium mixing ratio when surface emission fluxes are higher. Trace gases in H<sub>2</sub> atmospheres with low UV irradiation can easily accumulate (e.g., Seager et al. 2013), which further amplifies the difference between the two scenarios.

We demonstrate the difference between our high and low outgassing scenarios and the ability of JWST to differentiate them in Figure 5, assuming one NIRSpec Prism transit. CH<sub>4</sub> accumulates to very high levels in the cool (4000 and 5000 K) WD models for reasons we will discuss in Section 3.4. As a result, the high and low outgassing scenarios can be differentiated at  $\sim 3\sigma$  and  $>5\sigma$  in the 4000 K and 5000 K models, respectively, based on several CH<sub>4</sub> features in 1.0–2.5  $\mu\text{m}$ . For the 6000 K WD model, CO<sub>2</sub> features at 2.8 and 4.2  $\mu\text{m}$  and the CO feature at 4.7  $\mu\text{m}$  are the keys differences. Conclusive differentiation is not achievable for the 6000 K WD model with one NIRSpec Prism transit due to a low signal-to-noise ratio (S/N), but is achievable with five transits.

### 3.4. H<sub>2</sub>-dominated Atmospheres around WDs Can Test Photochemical Runaway

Gases whose major sinks are photochemical reaction powered by UV photons can potentially undergo so-called “photochemical runaway” in H<sub>2</sub>-dominated atmospheres around cool WDs. Photochemical runaway occurs when the emission of a gas saturates its photochemical sink. Under such conditions, trace species, such as biosignature gases, can accumulate to detectable levels (e.g., Segura et al. 2005; Sousa-Silva et al. 2020; Zhan et al. 2021; Ranjan et al. 2022). It is debated whether photochemical runaway is a physically realistic process or an artifact of photochemistry models. For a detailed quantitative exploration in support of the physicality of photochemical runaway, see Ranjan et al. (2022).

Photochemical runaway can occur on exoplanets around cool WDs because the UV-powered photochemical sinks can be easily saturated. UV photons generally play a key role in the photochemical removal of atmospheric gases for planets and moons in the solar system, either by dissociating molecules directly or by producing reactive radicals (e.g., Catling & Kasting 2017; Ranjan et al. 2022). As the effective temperature of a WD drops from 6000 K to 4000 K, UV radiation plummets by a factor of  $\sim 10^{10}$  (Figure 1).

Extremely low UV radiation from cool WDs implies that a physically plausible surface emission flux can trigger photochemical runaway. Indeed, runaway buildup is observed for CH<sub>4</sub>, CO<sub>2</sub>, and CO in our H<sub>2</sub>-dominated atmospheric models (Figure 2). Here we use CH<sub>4</sub> as an example to study

photochemical runaway in H<sub>2</sub> atmospheres around cool WDs, because CH<sub>4</sub> buildup has the strongest impact on transmission spectra. Rapid CH<sub>4</sub> buildup as  $T_{\text{eff}}$  of the host WD decreases agrees with previous studies assuming Earth-like atmospheres (Kozakis et al. 2018). Column-integrated mixing ratios of CH<sub>4</sub> are summarized in Table 2.

The nonlinear nature of photochemical runaway is observed in our models. Once past the runaway threshold, CH<sub>4</sub> increase is thought to increase drastically given a small increase in surface emission (Ranjan et al. 2022). Indeed, a 1000-fold increase in outgassing rate results in a  $\sim 10^6$  increase in CH<sub>4</sub> mixing ratio in our 4000 K WD H<sub>2</sub> atmospheric model. For comparison, the same increase only results in a  $\sim 100$  times increase in mixing ratio in the 5000 K WD model, which can be explained by a higher runaway threshold because a 5000 K WD produces higher UV radiation. In the 6000 K WD model, an increase in CH<sub>4</sub> outgassing rate results in a slight decrease in CH<sub>4</sub> mixing ratio. This is likely because outgassing rates of oxidizing gases such as CO<sub>2</sub> are increased by the same factor, and the supply of UV photons is sufficient to catalyze the reaction of CH<sub>4</sub> with oxidants. In other words, for  $>6000$  K, pCH<sub>4</sub> is limited by oxidant flux, not UV flux, as pO<sub>2</sub> is limited by reductant flux on modern Earth. Given the modern Sun-like UV radiation of a 6000 K WD, an increase in oxidizing gas emission has a stronger impact on the photochemical equilibrium than an increase in CH<sub>4</sub>.

Runaway buildup of CH<sub>4</sub> on transiting cool WD exoplanets also implies that spectral signatures of CH<sub>4</sub> are easily detectable. For H<sub>2</sub>-dominated models, one transit with NIRSpec Prism can detect CH<sub>4</sub> conclusively (Figure 5) for a hypothetical rocky planet orbiting WD 1856+534 in the WD HZ. For reference, Figure 6 shows the contribution of each important absorbing species to the overall transmission spectra. For the H<sub>2</sub> 6000 K scenario, models fit simulated observations very well at the 1.2 and 1.4  $\mu\text{m}$  CH<sub>4</sub> features, with the highest data points  $\sim 5\sigma$  from the baseline. The CH<sub>4</sub> feature at 3.4  $\mu\text{m}$  is also accessible despite larger error bars. The CH<sub>4</sub> feature at 2.3  $\mu\text{m}$ , however, overlaps with an H<sub>2</sub>-H<sub>2</sub> collision-induced absorption (CIA) feature and hence is challenging to detect. For the H<sub>2</sub> 5000 K scenario, the high CH<sub>4</sub> mixing ratio ( $4.2 \times 10^{-3}$ ) combined with the extended scale height of an H<sub>2</sub>-dominated atmosphere produce very strong CH<sub>4</sub> features for the high outgassing case. The strength of the features makes very high  $\sigma$  significance detection possible with one NIRSpec Prism transit, especially in the shorter wavelengths due to high S/N. For the H<sub>2</sub> 4000 K model, the runaway buildup of CH<sub>4</sub> that reaches a mixing ratio of 0.73 significantly changes the atmosphere’s MMW and shrinks its scale height. CH<sub>4</sub> features in the high outgassing model are weaker than in the 5000 K scenario, but still strong enough for  $>5\sigma$  detection. In the low outgassing model, CH<sub>4</sub> features are considerably weaker, but the highest data points at the 1.4  $\mu\text{m}$  feature are still  $\sim 3\sigma$  from the baseline.

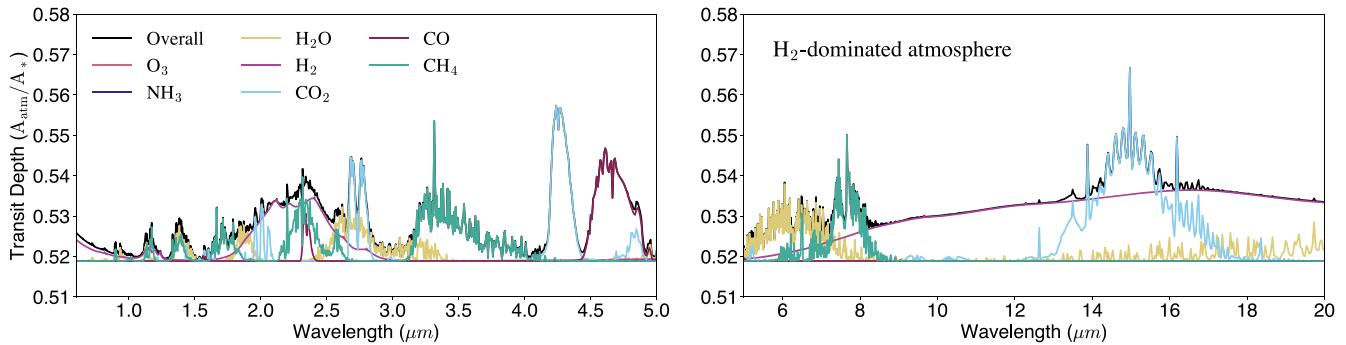


**Figure 6.** Molecular contributions to the overall model transmission spectra for  $\text{H}_2$ -dominated atmospheres. Only the 6000 K WD high outgassing rate scenario is shown for simplicity. The left panel shows features in the bandpass of NIRSpec Prism (0.6–5  $\mu\text{m}$ ) to allow for comparison with Figure 5, and the right panel shows infrared features in 5–20  $\mu\text{m}$ .

Our examination on  $\text{CH}_4$  is only a case study—photochemical runaway can occur for any gas with a high enough production rate to saturate its photochemical sink, which is usually powered by UV photons. The extremely low UV radiation of cool WDs means that many gases, including  $\text{CO}$ ,  $\text{PH}_3$ ,  $\text{NH}_3$ , and isoprene, can easily enter photochemical runaway (e.g., Ranjan et al. 2022). Among these gases,  $\text{PH}_3$ ,  $\text{NH}_3$ , and isoprene have been suggested as potential biosignatures (Sousa-Silva et al. 2020; Huang et al. 2021; Zhan et al. 2021), while  $\text{CH}_4$  in combination with  $\text{O}_2$  or  $\text{O}_3$  is considered a strong biosignature pair (e.g., Lederberg 1965). While we only consider volcanic emission, on habitable WD planets, additional biogenic emission may trigger photochemical runaway more easily. Therefore, transiting terrestrial WD exoplanets may be the most accessible targets for biosignature detection.

#### 4. Results for $\text{N}_2$ - and $\text{CO}_2$ -dominated Atmospheres

To explore more possible oxidation states of exoplanet atmospheres, we also run our photochemical model assuming  $\text{N}_2$ - and  $\text{CO}_2$ -dominated atmospheres. The key difference between these two high MMW atmospheric compositions and the  $\text{H}_2$ -dominated scenario is that a WD exoplanet with a high MMW atmosphere can either be first- or second-generation. Here we discuss why this degeneracy is unlikely to be resolved. Additional results for high MMW atmospheres, including outgassing activities, photochemical runaway, and location and detectability of transmission spectra features, are summarized in Appendix D.

Ambiguity in the formation origin comes from the high survivability of high MMW atmospheres. Both Jeans escape and energy-limited hydrodynamic escape have sensitive dependence on molecular weight. The Jeans escape flux  $\Phi_J \propto e^{-\lambda_J}$ , where  $\lambda_J$  is the Jeans escape parameter that is linearly dependent on molecular mass (e.g., Catling & Kasting 2017). Therefore, a 14-fold increase of MMW from a mass of  $\text{H}_2$  (2 amu) to  $\text{N}_2$  (28 amu) would result in an  $e^{-14}$  ( $\sim 10^{-7}$ ) decrease in Jeans escape flux. The decrease would be more drastic for  $\text{CO}_2$  (44 amu). Energy-limited escape of hydrogen can drag heavy molecules along with it.  $\text{H}_2$  mixing ratios in our  $\text{N}_2$ - and  $\text{CO}_2$ -dominated atmospheric models do not exceed  $\sim 10^{-3}$ , so even in the physically unlikely scenario that all hydrogen atoms are lost, and each H atom drags along an N or C atom, the impact of escape on the whole atmosphere is limited. The exact escape rate of heavy molecules, however, would depend on the mass of the heavy molecule, upward H escape flux, thermospheric temperature,

and hydrogen diffusion through a high MMW atmosphere (Luger & Barnes 2015). Quantitative constraints on hydrodynamic escape rates of heavy species is therefore beyond the scope of this work.

Even if a high MMW atmosphere is lost during the post-MS evolution, a rocky WD planet can potentially replenish the atmosphere via volcanic outgassing, adding another layer of uncertainty to the planet’s origin. Emission of oxidizing heavy molecules can continue at high rates on geological timescales.  $\text{CO}_2$ , for example, can be recycled from the atmosphere to sustain long-term high  $\text{CO}_2$  emission rates on an active lid planet (e.g., Kasting & Catling 2003).  $\text{N}_2$  is also produced from volcano arcs and mid-ocean ridges on Earth at a rate of  $\sim 10^8 \text{ cm}^{-2} \text{ s}^{-1}$  (Fischer 2008), and the geological nitrogen cycle appears to be well balanced by the interplay between volcanic emission and sedimentary burial (Catling & Kasting 2017). We therefore conclude that high MMW atmospheres dominated by  $\text{N}_2$  and  $\text{CO}_2$  can potentially be replenished after erosion.

Even though  $\text{N}_2$ - and  $\text{CO}_2$ -dominated atmospheres cannot uniquely constrain the evolutionary history of a rocky WD exoplanet, these high MMW atmospheres can be conclusively detected by JWST with a small number of transits. For most scenarios, even one transit with NIRSpec Prism can rule out a flat spectrum and hence imply the presence of an atmosphere with high significance (Table 1). Assuming high outgassing rates, flat spectra can be ruled out conclusively for  $\text{N}_2$  5000 K WD,  $\text{N}_2$  6000 K WD,  $\text{CO}_2$  4000 K WD, and  $\text{CO}_2$  5000 K WD scenarios at  $\gtrsim 5\sigma$ . For the low outgassing models, a barren rock planet can be ruled out at  $>3\sigma$  for all cases, despite weaker spectral features due to reduced emissions. We note two exceptions—the high outgassing  $\text{N}_2$  4000 K WD and  $\text{CO}_2$  6000 K WD models have low significance of  $2.7\sigma$  and  $2.3\sigma$ , respectively. This deviation from the general trend can be explained by stochastic noises added to each PandExo simulation. Our simulated JWST observations represent a set of *random* samples, rather than a set of *typical* samples. Fluctuations in calculated significance are therefore normal.

With five NIRSpec Prism transits, conclusive ( $>5\sigma$ ) detection is achievable for almost all scenarios for a hypothetical rocky planet orbiting WD 1856+534 in the WD HZ. There are two exceptions,  $\text{N}_2$  5000 K WD and  $\text{CO}_2$  4000 K WD scenarios, where the significance of ruling out a flat spectrum with five transits is lower than the significance with one transit. Because other models with similar transit depths have a very high significance of ruling out a flat spectrum ranging from  $6.5\sigma$  to  $7.8\sigma$ , we conclude that these two cases represent the pessimistic end of stochastic distribution of

PandExo noises. For a typical observation, JWST would be able to conclusively detect an  $N_2$  or  $CO_2$  atmosphere with five or fewer transits.

## 5. Discussion

### 5.1. $H_2$ Escape Mechanisms

Atmospheric loss driven by red-giant stellar winds has been quantitatively studied for  $\sim 0.5 M_\oplus$  exomoons, Earth-mass planets, and  $>5 M_\oplus$  super-Earths (Ramirez & Kaltenegger 2016). The authors considered Earth-like high MMW atmospheres and concluded that  $\sim 100\%$  atmospheric loss will occur for planets receiving Mars-like stellar radiation orbiting F5 or later type stars, when the host stars evolve into red giants. For K5 or later type MS progenitors, even a Saturn equivalent separation cannot prevent total atmospheric loss. Due to the complex nature of turbulent mixing, efficiency of atmospheric loss due to interactions with stellar winds is not well constrained, so we leave quantitative study of  $H_2$  atmosphere survivability around red giants for future investigation.

Note that present-day WDs cannot have originated from M dwarfs, because MS lifespans of M dwarfs are considerably longer than the age of the universe. Therefore, escape mechanisms specific to M dwarfs such as ion escape (e.g., Airapetian et al. 2017; Dong et al. 2017) do not apply to WD exoplanets.

### 5.2. $H_2$ Production and Retention Mechanisms

Because rates of volcanic  $H_2$  emissions have been quantitatively discussed in Section 3.1, here we focus on outgassing during accretion (e.g., Elkins-Tanton & Seager 2008). A modeling study on various types of common meteorites has shown that a substantial  $H_2$ -dominated atmosphere can be outgassed via the reaction between water and metallic iron, if sufficient water is added to reduced meteoritic materials (Elkins-Tanton & Seager 2008). Further studies on mixtures of meteoritic materials showed that  $H_2$  would be the dominant form of hydrogen outgassing when oxygen fugacity (a measurement for rock oxidation state) of the mixture is roughly lower than or equal to the oxidation state of O chondrites (e.g., Schaefer & Fegley 2010).

Compositional study of WD pollutants, which represent the building blocks for second-generation WD exoplanets, implies that second-generation rocky WD planets are capable of outgassing substantial  $H_2$ . WD pollutants are similar to solar system meteorites in bulk elemental composition and oxygen fugacity (Doyle et al. 2019). Measured oxygen fugacity of planetary materials accreted by six polluted WDs is consistent with C chondrites, O chondrites, bulk Earth, and bulk Mars. This compositional similarity implies that at least some second-generation planets formed from WD debris disks have Earth- and Mars-like geophysical and geochemical properties (Doyle et al. 2019). Both Earth and Mars are thought to have had an early  $H_2$ -rich phase (e.g., Ramirez et al. 2014), so it is not surprising if a geochemically similar second-generation rocky WD planet is born with a hydrogen envelope.

The addition of water to a forming second-generation rocky WD planet will facilitate  $H_2$  emission (Elkins-Tanton & Seager 2008), and water is indeed available in large quantities in WD debris disks. Observations of polluted WDs have shown that accreted materials can consist of 20% or more water by mass (e.g., Farihi et al. 2016), in agreement with model

predictions that water in minor planets or exomoons can survive post-MS evolution in large quantities (e.g., Malamud & Perets 2017). Accretion of such water-rich minor planets or comets onto a second-generation WD planet may yield a water reservoir equivalent to  $10^{-5}$ – $10^{-2}$  times the mass of Earth's ocean (Veras et al. 2014; van Lieshout et al. 2018). The initial water content of a second-generation WD planet may be enhanced if it accreted a tidally disrupted water-rich super-Earth. How much water can a second-generation planet recycle from the water-rich debris disk, however, remains an open question.

Kite et al. (2019, 2020) proposed that the abundance of 2–3  $R_\oplus$  sub-Neptunes can be explained by  $H_2$  dissolving into a long-lived magma ocean under excessive pressure. When  $H_2$  atmospheres suffer from atmospheric loss on such planets, hydrogen exsolution from the magma ocean can increase the survivability of  $H_2$  envelopes. Therefore, our results cannot be directly adopted to indicate the second-generation origin of  $H_2$ -rich sub-Neptunes. Nevertheless, planets considered by Kite et al. (2019, 2020) are in a completely different physical regime ( $\gtrsim 4 M_\oplus$  planets with  $\gtrsim 400$  K equilibrium temperature) compared to the temperate  $1 M_\oplus$  rocky planets we consider, so magma-atmosphere interaction does not affect our results.

### 5.3. Origin of Close-in Orbits of WD Exoplanets

We consider planets that receive similar irradiation as the Earth. Due to the low luminosity of WDs, these planets need to be in or near the WD HZ ( $\sim 0.005$ – $0.01$  au) to receive sufficient heating (Agol 2011). The origin of such close-in orbits needs to be accounted for.

Second-generation WD planets naturally have close-in orbits because they form at the 2:1 mean motion resonance with the WD Roche limit. Coincidentally, the 2:1 resonance fits in the HZ of  $T_{\text{eff}} \lesssim 6000$  K WDs (van Lieshout et al. 2018).

First-generation planets, however, must be delivered into a close-in orbit by some migration mechanism, because any first-generation planets born close to the star would be engulfed in the red-giant phase. There are two mechanisms that can deliver a remote planet to close-in orbits around WDs, namely binary star system interactions and multi-planet scattering. In a wide binary stellar system, the distant stellar companion can perturb the orbit of a major planet orbiting the evolving post-MS star and potentially deliver it into the Roche limit of its host. Under this mechanism, Neptune-like planets or Kuiper Belt analog objects would spend the first  $\sim 200$  Myr of the WD lifetime of their host on a  $\sim 100$  au orbit. Subsequently, the planet can be delivered to a close-in orbit with  $\sim 10^{-2}$  au periapsis by relatively rapid inward migration that takes  $\sim 5$  Myr (Stephan et al. 2017). Alternatively, in a closely packed multi-planet system, due to the chaotic nature of scattering, a planet can remain on a  $\sim 10$  au orbit for  $>10$  Gyr and then be scattered onto a highly eccentric orbit with periapsis distance of only a few percent of an astronomical unit (Veras & Gänsicke 2015). Tidal interactions with the WD can then circularize its orbit in under 1000 yr. Efficient tidal interaction also means that planets in WD HZ are tidally locked (e.g., Agol 2011).

### 5.4. Clouds and Hazes in WD Exoplanet Atmosphere

Pervasive high cloud decks pose a major challenge to the detection of spectral features, because molecules below cloud decks are not accessible. Recent general circulation model

(GCM) simulations concluded that transit observations of tidally locked M dwarf terrestrial exoplanets, especially water-rich planets, would be strongly affected by clouds (Komacek et al. 2020; Suissa et al. 2020). In the moist greenhouse regime, however, highly saturated stratosphere improves the detectability of H<sub>2</sub>O despite thick tropospheric clouds (Chen et al. 2019). Clouds also affect our photochemistry models indirectly by controlling the atmospheric energy budget and by influencing the amount of UV reaching the lower atmosphere. Planets in WD HZs are rapid rotators with  $\approx 4\text{--}32$  hr periods (Agol 2011), in contrast to the slowly rotating ( $\gtrsim 12$  days) M dwarf planets on which cloud effects are most pronounced (Komacek et al. 2020).

Our photochemistry models imply that strong haze formation may be prevalent in the atmospheres of WD exoplanets. In an Archean Earth-like N<sub>2</sub>-dominated anoxic atmosphere, a CH<sub>4</sub>/CO<sub>2</sub> ratio of above 0.1 would lead to strong hydrocarbon haze production driven by CH<sub>4</sub> photolysis (e.g., Arney et al. 2016). Indeed, our photochemistry results show that in N<sub>2</sub>-dominated models with high outgassing rates, CH<sub>4</sub>/CO<sub>2</sub> equals 0.72, 1.0, and 5.9 for 6000 K, 5000 K, and 4000 K WDs, respectively. In N<sub>2</sub>-dominated models with low outgassing rates, CH<sub>4</sub>/CO<sub>2</sub> ratios are  $6.2 \times 10^{-6}$ ,  $1.4 \times 10^{-6}$ , and 1.0 for 6000 K, 5000 K, and 4000 K WDs, respectively. Given the high CH<sub>4</sub>/CO<sub>2</sub> ratios for all high outgassing scenarios and the 4000 K low outgassing scenario, extensive organic haze production in the atmospheres of WD exoplanets may be common.

Even though the production of organic hazes in CO<sub>2</sub>- and H<sub>2</sub>-dominated atmospheres is not well studied, CH<sub>4</sub>/CO<sub>2</sub> ratios in our photochemistry models for these types of atmospheres often exceed 0.1. In a CO<sub>2</sub>-dominated atmosphere with high outgassing rates, CH<sub>4</sub>/CO<sub>2</sub> equals  $4.3 \times 10^{-8}$ ,  $8.1 \times 10^{-6}$ , and 0.13 for 6000 K, 5000 K, and 4000 K WDs, respectively. In an H<sub>2</sub>-dominated atmosphere with high outgassing rates, CH<sub>4</sub>/CO<sub>2</sub> equals 0.13, 41, and  $2.3 \times 10^4$  for 6000 K, 5000 K, and 4000 K WDs, respectively. If haze production is also positively correlated with the CH<sub>4</sub>/CO<sub>2</sub> ratio in highly reducing or highly oxidizing atmospheres, the high CH<sub>4</sub>/CO<sub>2</sub> ratios for H<sub>2</sub>-dominated models and for the 4000 K WD CO<sub>2</sub>-dominated model imply that organic hazes on WD exoplanets are common regardless of atmospheric oxidation state.

Scattering from hazes can complicate detectability of spectral features, but the presence of hazes also provides a new approach to characterize the atmospheres of WD exoplanets and can even indicate biological activity. At visible wavelengths, scattering from hazes produces a slope at  $\sim 0.5 \mu\text{m}$  and shorter wavelengths (e.g., Marley et al. 2013), which has a similar shape compared to the Rayleigh scattering slope. In an atmosphere with an Earth-like concentration of oxygenic species, such haze slopes may also obscure the O<sub>3</sub> Chappuis band at  $0.6 \mu\text{m}$ , complicating the detection of the CH<sub>4</sub> + O<sub>3</sub> biosignature pair (e.g., Lin et al. 2021). In infrared wavelengths, organic haze has a feature at approximately  $6 \mu\text{m}$ , just outside of the bandpass of NIRSpec Prism (Arney et al. 2016, 2017). If organic haze features are detected on a WD exoplanet with a low CH<sub>4</sub>/CO<sub>2</sub> ratio, it is possible that the planet has large emissions of biogenic sulfur gases (Arney et al. 2018).

### 5.5. Habitability of WD Exoplanets

Here we discuss how the changing luminosity, UV radiation, volatile reservoir, and orbital dynamics would affect the habitability of WD exoplanets.

The slow cooling process of WDs provides stable environments for planets around them for billions of years. Agol (2011) estimated that a planet can stay in the continuously HZ of WDs for  $>3$  Gyr. Kozakis et al. (2018) showed that the maximum time a planet spends within the WD HZ of a  $0.6 M_{\odot}$  WD is  $\sim 6$  Gyr, assuming a conservative HZ defined by the runaway greenhouse effect and maximum greenhouse effect of H<sub>2</sub>O and CO<sub>2</sub> (e.g., Kasting et al. 1993). Furthermore, cool single WDs are photometrically stable (Fontaine & Brassard 2008), which rules out high-energy flares that may cause atmospheric erosion. Flares, which impact the habitability of M dwarf planets, should not affect WD planets we consider.

WDs remain cool and quiescent during most of their lifetime, providing a stable low UV environment for any planet orbiting it. High-energy UV photons can potentially erode atmospheres and place the water reservoir at risk, due to the photodissociation of water and subsequent hydrogen escape (e.g., Airapetian et al. 2017; Dong et al. 2017). Some studies have suggested that high UV flux may be necessary for triggering complicated prebiotic chemistry reactions, which are essential for the emergence of life (e.g., Fossati et al. 2012; Ranjan et al. 2018). WDs with  $T_{\text{eff}} = 6000$  K have UV radiation comparable to the modern Sun (Figure 1), implying that younger, hotter WDs can output UV photons on the same levels as the young Sun, which is presumed to trigger abiogenesis on Earth.

A rocky WD exoplanet can have an abundant volatile reservoir, which is another requirement for habitability. First-generation rocky WD planets may require either some migration mechanism that delivers the planet from an outer orbit into the WD HZ (e.g., Veras & Gänsicke 2015), or a large initial water fraction. In the latter case, steam-dominated atmospheres on water-rich “super-Venuses” can survive for geologic timescale even when exposed to intense EUV fluxes (Harman et al. 2021). Analogous to planets with high MMW atmospheres considered here, transiting WD planets with steam atmospheres can be readily characterized by JWST, offering an opportunity to study the volatile evolution on terrestrial planets. For a second-generation WD planet, whether it has sufficient volatiles depends on whether the WD debris disk from which the planet formed is volatile-rich. As discussed in Section 5.2, volatiles such as H<sub>2</sub>O are indeed abundant in WD debris disks, according to WD pollution observations.

Short tidal circularization and tidal locking timescales imply that planets in the WD HZ are expected to be tidally locked, with orbital periods of  $\approx 4\text{--}32$  hr (Agol 2011). Rapid rotation allows for efficient heat redistribution, preventing nighttime atmospheric collapse and hence increasing habitability. Rapid rotation also leads to the formation of narrow global cloud bands, in contrast to thick substellar cloud decks on slowly rotating planets, which have secondary effects on habitability that are explored by GCMs (e.g., Yang et al. 2014).

### 5.6. Future Opportunities

To date, no Earth-mass transiting WD planet has been discovered. Earth-sized rocky exoplanets transiting a cool WD in the HZ have transit durations of only  $\sim 2$  minutes, so

detection of such planets require high-cadence observations. Some have searched for such planets using both ground- and space-based facilities (e.g., van Sluijs & Van Eylen 2018). In addition, the feasibility of discovering WD exoplanets has been studied for astrometric detection by Gaia (Perryman et al. 2014) and for large-scale survey detection by the Large Synoptic Survey Telescope (LSST; Cortés & Kipping 2019). The new 20 s cadence mode available during the TESS extended mission will provide another avenue of detecting transiting WD exoplanets with short transit durations.

The search for Earth-mass transiting WD exoplanets may be a fruitful one. About five Earth-mass transiting WD exoplanets are expected to be detected within the characterization horizon of JWST, assuming Earth-like atmospheres (Kaltenegger et al. 2020). For H<sub>2</sub> atmospheres, the characterization horizon may be extended. The half-sky survey by LSST may produce a more optimistic number of  $\sim 100$  transiting WD exoplanets (Cortés & Kipping 2019), although some of those targets may be too dim for JWST to characterize.

## 6. Conclusion

In this work, we present a photochemical modeling exploration of Earth-mass exoplanets transiting WDs under the context of WD system evolution. We present 1D photochemistry models coupled with an analytical climate model, simulated transmission spectra, and JWST observation models for three types of anoxic atmospheres with different oxidation states. We show that detection of an H<sub>2</sub>-dominated thick ( $\sim 1$  bar) atmosphere indicates a second-generation WD rocky planet, while the detection of a high MMW (N<sub>2</sub>- or CO<sub>2</sub>-dominated) atmosphere is degenerate. Detecting H<sub>2</sub>O, H<sub>2</sub>, CO<sub>2</sub>, CO, and CH<sub>4</sub> features in H<sub>2</sub> atmospheres with JWST requires only one transit with NIRSpec Prism. For N<sub>2</sub>- and CO<sub>2</sub>-dominated atmospheres,  $\sim 25$  NIRSpec Prism transits are required to conclusively detect the above molecules. Buildup of CH<sub>4</sub> via photochemical runaway is observed in most models, an effect that can be used to differentiate between high and low outgassing scenarios with one JWST transit for H<sub>2</sub> atmospheric models and with 25 JWST transits for most N<sub>2</sub> and CO<sub>2</sub> atmospheric models. For more details on molecule detectability in H<sub>2</sub>-dominated atmospheres, see Appendix C. For additional results and figures for N<sub>2</sub>- and CO<sub>2</sub>-dominated atmospheres, see Appendix D.

Earth-mass transiting WD exoplanets are among the most favorable targets for atmospheric characterization of terrestrial planets via transmission spectroscopy. Besides an opportunity to search for biosignature gases on inhabited WD exoplanets, here we show that there is also a “white dwarf opportunity” for constraining the evolutionary history of abiotic and prebiotic rocky WD exoplanets. Rocky exoplanets transiting WDs are yet to be found. We intend for the results here to motivate the search for these unique worlds circling dead stars and follow-up atmospheric reconnaissance by JWST.

We thank the anonymous reviewer for constructive comments that improved the clarity of this paper. We thank Sujun Sengupta for co-developing a hydrogen escape code that contributed to this study. Z.L. acknowledges support from the MIT Presidential Fellowship. S. R. thanks Northwestern University for support via the CIERA Postdoctoral Fellowship.

## Appendix A Model Details

### A.1. Photochemistry Model

Our photochemistry model includes  $>800$  chemical reactions, photochemical processes, and emission and thermal escape mechanisms. The model also solves chemical-transport equations for 111 O, H, C, N, and S species, as well as S<sub>8</sub> and H<sub>2</sub>SO<sub>4</sub> aerosols, linked by 645 bimolecular reactions, 85 termolecular reactions, and 93 thermal dissociation reactions (see Hu et al. 2012 for a full list of species and reactions). The reaction network has recently been updated to include nitrogenous chemistry, and the rate laws of several reactions have been updated as well (see Ranjan et al. 2022). Note that because photochemistry of higher hydrocarbons and organic haze production involves many uncertainties, Hu et al. (2012) excluded reactions involving molecules containing more than two carbon atoms in an ad hoc fashion by assuming a high ( $10^{-5}$  cm s<sup>-1</sup>) deposition velocity for C<sub>2</sub>H<sub>6</sub>. Implications of hazy atmospheres are discussed in Section 5.4.

For each atmospheric oxidation state, we use a subset of the full reaction network that is relevant. We assume the planets are covered with a substantial surface liquid water ocean and water vapor is transported upwards at a constant flux of  $10^{-2}$  cm<sup>-2</sup> s<sup>-1</sup> due to evaporation. We consider a zero rainout rate to simulate an ocean that is saturated with H<sub>2</sub>, CO, CH<sub>4</sub>, C<sub>2</sub>H<sub>6</sub>, and O<sub>2</sub> on an abiotic planet (following Hu et al. 2012). Dry deposition velocities assumed in our model follow the exoplanet benchmark case parameters (see Table 5 of Hu et al. 2012). The photochemical model is considered to be converged when the variation timescale of each species at each altitude exceeds the diffusion timescale of the entire atmosphere. Key model parameters are summarized in Table 3.

Our high and low outgassing rates differ by a factor of 1000. This factor is not arbitrary. The volcanic production rate of modern Earth is  $\sim 100$ – $1000$  times higher than that of Venus (Gaillard & Scaillet 2014; Gillmann & Tackley 2014). To explore a wider parameter space, we choose a factor of 1000 instead of 100.

The required inputs of the temperature model include the planet’s equilibrium temperature, interior temperature, mean thermal opacity of the atmosphere, and mean optical opacity. Equilibrium temperatures of our models are summarized in Table 3. For all models, we assume an Earth-like interior temperature of 35.7 K, which is calculated based on an estimated total surface heat flow of Earth of  $47 \pm 2 \times 10^{12}$  W (Davies & Davies 2010). Mean thermal and optical opacities were calculated based on mixing ratios of key absorbing species, such as CH<sub>4</sub>, CO<sub>2</sub>, H<sub>2</sub>O, and H<sub>2</sub>, produced by the photochemistry model, in combination with cross-sectional data from the Exoclines Simulation Platform (Grimm & Heng 2015) and the MPI-Mainz Spectral Atlas (Keller-Rudek et al. 2013). Opacities calculated from photochemistry model outputs are inputted to the temperature model as initial conditions, while the temperature–pressure profile generated by the temperature model is in turn inputted to the photochemistry model. The two models were run iteratively until the surface temperature predicted by both models differs by less than 1 K. We run several extra iterations after convergence to ensure a stable solution. Surface temperatures for all three 6000 K WD models are fixed at 288 K, and the thermal and optical opacities of the 6000 K WD models were used as benchmarks for the 5000 K and 4000 K WD models. The cooler

**Table 3**  
Model Parameters for the Three Anoxic Atmospheric Compositions

Parameters		Reducing (90% H <sub>2</sub> , 10% N <sub>2</sub> )		Weakly Oxidizing (>99% N <sub>2</sub> )		Highly Oxidizing (90% CO <sub>2</sub> , 10% N <sub>2</sub> )	
		High	Low	High	Low	High	Low
Outgassing scenario							
Equivalent semimajor axis (au)		1.6	1.6	1.0	1.0	1.3	1.3
Mass ( $M_{\oplus}$ )		1.0	1.0	1.0	1.0	1.0	1.0
Radius ( $R_{\oplus}$ )		1.0	1.0	1.0	1.0	1.0	1.0
Surface pressure (bar)		1.0	1.0	1.0	1.0	1.0	1.0
Surface temperature (K)	4000 K WD	347	288	299	284	290	288
	5000 K WD	290	288	289	284	288	288
	6000 K WD	288	288	288	284	288	288
MMW (amu)	4000 K WD	13	4.6	28	28	39	42
	5000 K WD	4.7	4.6	28	28	42	42
	6000 K WD	4.6	4.6	28	28	42	42
Gas emission(cm <sup>-2</sup> s <sup>-1</sup> )	CO <sub>2</sub>	$3 \times 10^{11}$	$3 \times 10^8$	$3 \times 10^{11}$	$3 \times 10^8$	N/A	N/A
	H <sub>2</sub>	N/A	N/A	$3 \times 10^{10}$	$3 \times 10^7$	$3 \times 10^{10}$	$3 \times 10^7$
	SO <sub>2</sub>	$3 \times 10^9$	$3 \times 10^6$	$3 \times 10^9$	$3 \times 10^6$	$3 \times 10^9$	$3 \times 10^6$
	CH <sub>4</sub>	$3 \times 10^8$	$3 \times 10^5$	$3 \times 10^8$	$3 \times 10^5$	$3 \times 10^8$	$3 \times 10^5$
	H <sub>2</sub> S	$3 \times 10^8$	$3 \times 10^5$	$3 \times 10^8$	$3 \times 10^5$	$3 \times 10^8$	$3 \times 10^5$
Water and rainout	f(H <sub>2</sub> O) surface emission	0.01	0.01	0.01	0.01	0.01	0.01
	rainout rate	0	0	0	0	0	0

WD models have a higher concentration of gases with high thermal opacities due to lower UV radiation from host stars and hence lower photodissociation rate. This would increase the thermal opacities of cooler WD models relative to the 6000 K WD model, causing temperatures to increase. The final converged surface temperatures for all of the models are summarized in Table 3.

### A.2. Transmission Spectra Model

Our transmission spectra model includes the most spectroscopically relevant species: C<sub>2</sub>, C<sub>2</sub>H<sub>2</sub>, C<sub>2</sub>H<sub>4</sub>, CH, CH<sub>3</sub>, CH<sub>4</sub>, CN, CO, CO<sub>2</sub>, CS, H<sub>2</sub>, H<sub>2</sub>O, H<sub>2</sub>O<sub>2</sub>, H<sub>2</sub>S, HCN, HNO<sub>3</sub>, NH, NH<sub>3</sub>, O<sub>3</sub>, OH, SO<sub>2</sub>, and SO<sub>3</sub>. We include the following Rayleigh scattering species: H<sub>2</sub>O, CO, CH<sub>4</sub>, CO<sub>2</sub>, H<sub>2</sub>, O<sub>2</sub>, and N<sub>2</sub>. Collision-induced absorption (CIA) plays an important role in transmission spectroscopy, especially when one or both species in a CIA pair exist in a high concentration in the modeled atmosphere. We therefore include the following CIA pairs: N<sub>2</sub>-N<sub>2</sub>, H<sub>2</sub>-H<sub>2</sub>, O<sub>2</sub>-O<sub>2</sub>, N<sub>2</sub>-O<sub>2</sub>, CO<sub>2</sub>-CO<sub>2</sub>, and H<sub>2</sub>-He.

A detailed vertical and horizontal distribution of realistic 3D clouds on exoplanets is highly uncertain. For generality, we assume a single homogeneous cloud layer located at 6 km in the N<sub>2</sub>-dominated atmosphere (following Lin et al. 2021). For consistency across atmospheres with different scale heights, we place the cloud layer at 0.47 bar in the CO<sub>2</sub>- and H<sub>2</sub>-dominated models, which corresponds to 6 km in the N<sub>2</sub>-dominated atmospheres. We account for the most pessimistic scenario by assuming the cloud layer is fully opaque and covers the entire day-night terminator.

The effect of atmospheric refraction is dependent on  $R_*/a$ , the inverse of the scaled semimajor axis, and is strongest when this value is small (Bétrémieux & Kaltenegger 2014; Robinson et al. 2017). Applying Equation (14) from Robinson et al. (2017), we find that the maximum pressures accessible to transmission spectroscopy are  $\approx 0.7$ ,  $\approx 4$ , and  $\approx 0.3$  bar, for N<sub>2</sub>, H<sub>2</sub>, and CO<sub>2</sub> atmospheres, respectively, with uncertainties coming from the

exact choice of orbital distance, MMW, and atmospheric refractivity. The refractive cutoffs in N<sub>2</sub>- and H<sub>2</sub>-dominated atmospheres are below the cloud layer at 0.47 bar and therefore do not affect the transmission spectra. The refractive cutoff in a CO<sub>2</sub>-dominated atmosphere, however, is above the cloud deck, so we introduce a completely opaque layer at 0.3 bar.

## Appendix B

### Quantitative Analysis of H<sub>2</sub>-dominated Atmospheres as an Indicator of Second-generation Planets

#### B.1. Survivability of Hydrogen Atmospheres on First-generation WD Exoplanets

In this section, we quantitatively discuss hydrogen escape on a first-generation rocky planet during the hot WD phase. We show that even if the planet migrates to a 50–100 au orbit, excessive EUV radiation from the hot WD can lead to complete erosion of a  $\sim 1$  bar hydrogen atmosphere.

Two types of neutral atmospheric escapes are relevant for rocky planets, namely Jeans escape and hydrodynamic escape. Hydrodynamic escape dominates at high incident fluxes and can produce extremely high mass-loss rates that can account for the evaporation of entire atmospheres (Owen & Wu 2013). We therefore focus on the hydrodynamic escape mechanism and calculate the “energy-limited” mass-loss rate given the EUV irradiation from a hot WD.

Intense EUV radiation from hot WDs results in extreme mass-loss rates. EUV flux from a hot ( $\gtrsim 30,000$  K) WD exceeds EUV flux of the young Sun by a factor of  $10^2$ – $10^3$ , while the young Sun is thought to have been  $10^3$  times more active than the modern Sun (Schreiber et al. 2019). Even at a distance of  $\sim 50$ – $100$  au, EUV flux from a 40,000–80,000 K WD can be as strong as  $\sim 0.1$ – $10$  W m<sup>-2</sup>. In this EUV flux range, atmospheric escape is dominated by the so-called “energy-limited” escape (e.g., Luger & Barnes 2015; Sengupta 2016). Here we adopt Equation (2) in Luger & Barnes (2015) to calculate the mass-

loss rate on rocky exoplanets orbiting hot WDs:

$$\dot{M}_{\text{EL}} = \frac{\epsilon_{\text{EUV}} \pi \mathcal{F}_{\text{EUV}} R_p R_{\text{EUV}}^2}{GM_p K_{\text{tide}}} \quad (1)$$

where  $\mathcal{F}_{\text{EUV}}$  is the EUV flux,  $R_p$  is the planet radius,  $R_{\text{EUV}}$  is the radius at which the bulk of EUV energy is deposited,  $\epsilon_{\text{EUV}}$  is the EUV absorption efficiency, and  $K_{\text{tide}}$  is the tidal correction term. We make several simplifications here:  $R_{\text{EUV}}$  is assumed to be equal to  $R_p$  because scale height  $H \ll R_p$  on a rocky planet,  $\epsilon_{\text{EUV}}$  is assumed to be 0.3, and  $K_{\text{tide}}$  is assumed to be 1 (following Luger & Barnes 2015). We assume a  $1 R_{\oplus}$  radius and  $1 M_{\oplus}$  mass. We consider the scenario that the planet migrates to a  $\sim 50$ – $100$  au orbit around a  $\sim 40,000$  K WD, which is optimistic for hydrogen survival. EUV flux received by the planet in this case is assumed to be  $0.1 \text{ W m}^{-2}$  (following Schreiber et al. 2019). Hydrogen escape flux in this scenario is  $4.1 \times 10^7 \text{ kg s}^{-1}$ , which is equivalent to  $2.4 \times 10^{31}$  H atoms per second. In addition, we perform a sensitivity test assuming different values of  $\epsilon_{\text{EUV}}$  and  $R_{\text{EUV}}$ . Luger & Barnes (2015) considered  $0.15 \leq \epsilon_{\text{EUV}} \leq 0.3$  as typical for  $\text{H}_2$ -rich atmospheres. Our model  $\text{H}_2$  atmospheres have maximum altitudes of  $\sim 1200$  km, and we choose half of the maximum altitude (600 km) as the maximum  $R_{\text{EUV}}$ . Pressures at 600 km in our models are  $\sim 10^6$  times lower than Earth’s exobase pressure. The sensitivity test results in a factor of  $\approx 2.4$  change in the energy-limited escape rate (Figure 4).

A first-generation WD planet can maintain its  $\text{H}_2$ -dominated atmosphere if sources of hydrogen overwhelm sinks. We make a first-order assumption that the sole sink for hydrogen is escape at the top of the atmosphere, and the sole source is volcanic emission. We consider an optimistic case that  $\text{H}_2$  outgassing is 20 times higher than modern Earth volcanic emission. The volcanic  $\text{H}_2$  flux on modern Earth is estimated to be  $1.5 \times 10^9 \text{ cm}^{-2} \text{ s}^{-1}$  (James & Hu 2018). On young planets with more reduced mantles or planets with additional internal heating due to tidal dissipation,  $\sim 20$  times higher production is plausible. We therefore assume  $3.0 \times 10^{10} \text{ cm}^{-2} \text{ s}^{-1}$  flux as a “high outgassing” scenario (following James & Hu 2018). We also consider a pessimistic “low outgassing” scenario where  $\text{H}_2$  outgassing is 1000 times lower than the high outgassing scenario. The high and low outgassing rates translate to global H atom production rates of  $3.1 \times 10^{29} \text{ s}^{-1}$  and  $3.1 \times 10^{26} \text{ s}^{-1}$  (Figure 4).

An immediate observation from Figure 4 is that even in the optimistic high outgassing scenario, hydrogen production is significantly less than hot WD EUV-driven hydrogen loss by a factor of  $\sim 100$ . Therefore, net  $\text{H}_2$  loss will occur even in the most optimistic scenario for hydrogen retention, where the planet migrates to a separation of  $\sim 50$ – $100$  au, orbits a relatively cool ( $\sim 40,000$  K) young WD, and emits 20 times more  $\text{H}_2$  than modern Earth. The mass-loss rate in this scenario is  $\sim 4 \times 10^4 \text{ kg s}^{-1}$ , or  $\sim 10^{12} \text{ kg yr}^{-1}$ . The total mass of Earth’s atmosphere is on the order of  $\sim 10^{18} \text{ kg}$ , so an  $\text{H}_2$  atmosphere on an Earth-mass first-generation WD exoplanet will be evaporated entirely on a timescale of  $\sim 1$  Myr. This timescale is shorter than the  $\sim 10$  Myr cooling time for the effective temperature of a  $100,000$  K WD to drop to  $30,000$  K (Fontaine et al. 2001). Cooling below  $30,000$  K is much slower. It takes  $\sim 2$  Gyr to cool a WD to  $6000$  K (Bergeron et al. 2001; Fontaine et al. 2001), and

at this temperature, the WD still emits EUV radiation comparable to the modern Sun (Figure 1). The extended exposure to high levels of EUV photon flux guarantees total evaporation of hydrogen envelopes on first-generation rocky WD planets.

## B.2. Escape Mechanisms on Rocky WD Exoplanet

Here we quantitatively study the escape mechanisms on a rocky planet orbiting cool ( $T_{\text{eff}} \lesssim 5000$  K) WDs. We conclude that maintaining an  $\text{H}_2$ -dominated atmosphere around a cool WD is possible for planets with high outgassing rates and an Earth-like exobase temperature ( $T_{\text{exo}}$ ), or planets with low outgassing rates and a Venus- or Mars-like  $T_{\text{exo}}$ . We break down our quantitative analysis in the order of Jeans escape, energy-limited escape, and diffusion.  $\text{H}_2$  emission and escape fluxes are visualized in Figure 4.

On a planet with low EUV irradiation, Jeans escape is the dominant escape mechanism. Jeans escape is controlled by the Jeans escape parameter, which is inversely proportional to  $T_{\text{exo}}$  (Hunten 1973; Tian et al. 2008). At low exobase temperatures ( $T_{\text{exo}} \lesssim 1000$  K), Jeans escape flux is a very sensitive function of exobase temperature, where a  $\sim 300$  K decrease in  $T_{\text{exo}}$  can lead to a two-orders-of-magnitude decrease in Jeans escape flux.

It should be reasonable to assume that the  $T_{\text{exo}}$  on cool WD exoplanets with anoxic atmospheres is lower than Earth’s  $T_{\text{exo}}$ , despite the lack of model constraints. Earth’s exobase is heated by several mechanisms, including UV-induced photoionization and photodissociation of  $\text{CO}_2$ ,  $\text{N}_2$ ,  $\text{O}$ ,  $\text{O}_2$  and  $\text{O}_3$ , where the most efficient heat source among all mechanisms is photoionization and photodissociation of  $\text{O}_2$  (see, e.g., Kulikov et al. 2007 and references therein). In anoxic atmospheres, such as  $\text{CO}_2$ -dominated Venusian and Martian atmospheres,  $T_{\text{exo}}$  can be as low as  $275$  K and  $350$  K, respectively (de Pater & Lissauer 2001). For comparison, Earth’s exobase is heated to a temperature of  $\sim 1000$  K (e.g., Tian et al. 2008). Because exospheric heating is powered by UV,  $T_{\text{exo}}$  varies with stellar activity. Earth’s exobase temperature ranges from  $\approx 700$  K to  $\approx 1500$  K depending on solar activity, with some uncertainties from the assumed eddy diffusion coefficient (Roble et al. 1987). To explore a wide parameter space, we consider Jeans escape for three  $T_{\text{exo}}$ :  $1500$  K,  $700$  K, and  $350$  K. Note that all three types of atmospheres we consider are anoxic, and the EUV levels of cool WDs are significantly lower than that of the modern Sun, so even the  $700$  K “solar min” exobase temperature is likely to be an overestimate for cool WDs. But we stick with these temperature choices to account for  $\gtrsim 6000$  K WDs with roughly solar level UV radiation.

We calculate Jeans escape rates on WD exoplanets based on formalism derived by Hunten (1973) and Watson et al. (1981). The Jeans escape rates are shown in Figure 4 alongside with  $\text{H}_2$  emission rates for comparison. The high outgassing rate is  $\sim 3$  times higher than the “solar max” Jeans escape rate and  $\sim 100$  times higher than the “solar min” Jeans escape rate. The low  $\text{H}_2$  outgassing rate is lower than the “solar min” Jeans escape rate but is  $\sim 1000$  times higher than the Jeans escape rate assuming  $T_{\text{exo}} = 350$  K. The low  $\text{H}_2$  outgassing rate also is comparable to the energy-limited escape rate around a  $5000$  K WD, but is many orders of magnitudes higher than the energy-limited escape rate around a  $4000$  K WD. Given that even the “solar min” escape rate is likely an overestimate for cool WDs, we

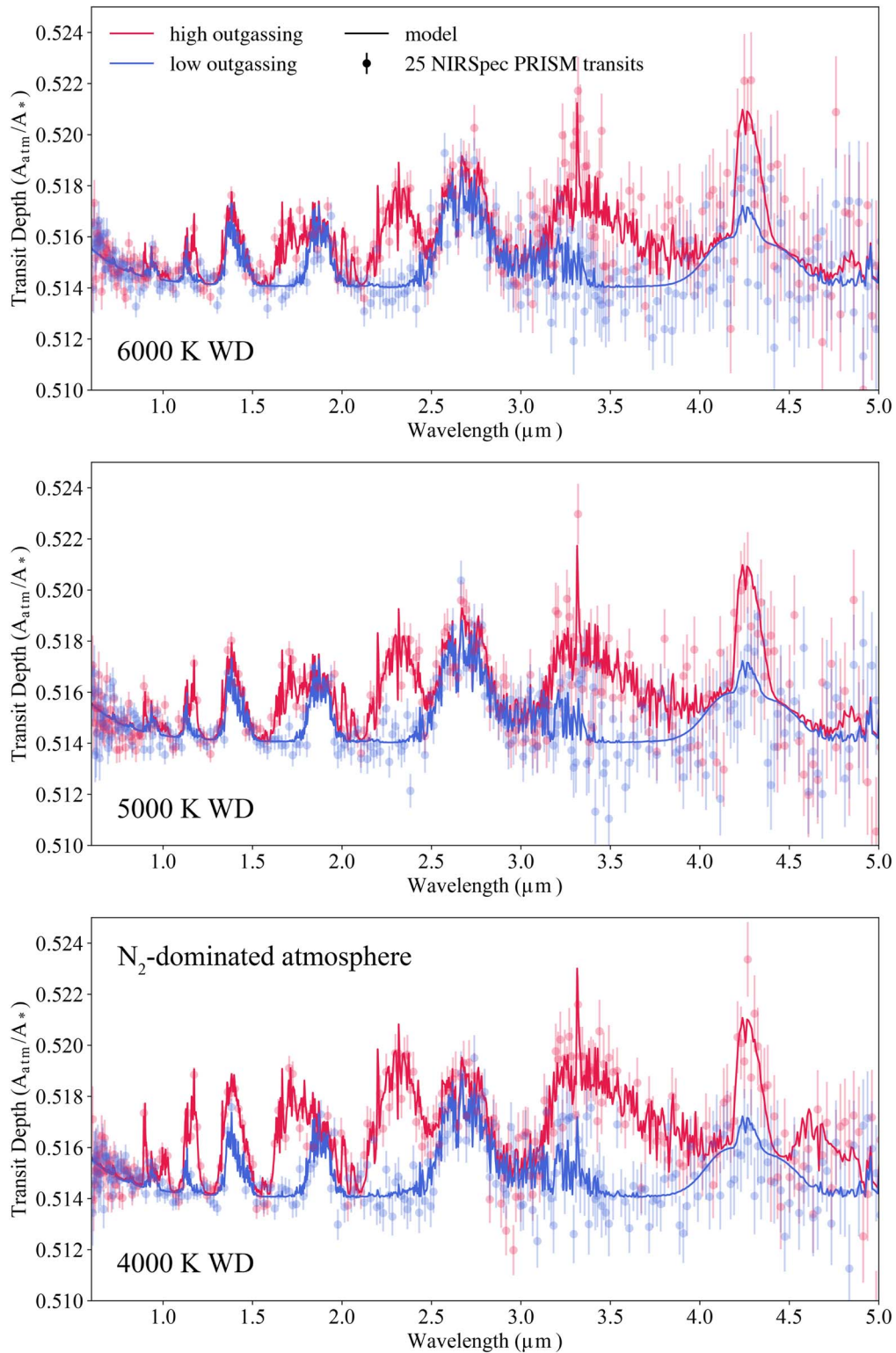


**Figure 7.** Transmission spectra models and simulated JWST transit observations for  $\text{N}_2$ -dominated atmospheres, assuming a  $1 R_{\oplus}$  planet transiting WD 1856+534. We compare high outgassing rate models (red solid lines) with low outgassing rate models (blue solid lines) and show simulated JWST data points with their  $1\sigma$  error bars. We assume 25 NIRSpec Prism transits for the  $\text{N}_2$ -dominated atmospheric models. Major spectral features are detectable in the  $\text{N}_2$ -dominated atmospheric models. High and low outgassing scenarios are potentially distinguishable from different strengths of  $\text{CH}_4$  features in all three models. In the 4000 K WD model, high and low outgassing scenarios are most easily distinguishable due to runaway buildup of  $\text{CH}_4$ .

conclude that a rocky planet around cool WDs can maintain a hydrogen atmosphere if it has modern Earth-like or higher  $\text{H}_2$  emissions. Even a planet with 1000 times reduced  $\text{H}_2$  emission can maintain an  $\text{H}_2$ -dominated atmosphere around a 4000 K

WD. Survival of an  $\text{H}_2$  atmosphere on a low outgassing planet orbiting a 5000 K WD would depend on the EUV levels of the particular WD and heating mechanisms in the planet's exosphere.

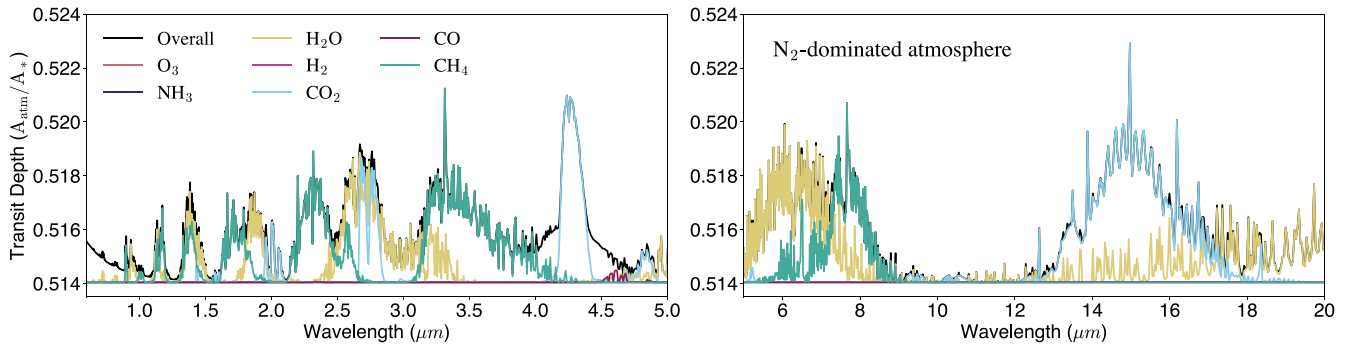


**Figure 8.** Molecular contributions to the overall model transmission spectra for  $N_2$ -dominated atmospheres.

Energy-limited hydrodynamic escape is important when EUV flux is high. In Figure 4, we show the energy-limited escape rate as a function of WD EUV radiation, following two analytical models (Luger & Barnes 2015; Sengupta 2016). Hydrogen escape flux due to energy-limited escape only becomes comparable to Jeans escape for  $\gtrsim 6000$  K WDs. Energy-limited escape flux drops logarithmically as EUV flux decreases and is orders-of-magnitudes lower than Jeans escape flux for  $\lesssim 5000$  K WDs and is therefore neglected.

On Earth, hydrogen escape is not limited by the rate at which H atoms diffuse into space, but rather by the rate at which hydrogen is delivered to the exobase from the collisional lower atmosphere (e.g., Catling & Kasting 2017). In an atmosphere where  $H_2$  is the dominant constituent, however, the supply of hydrogen is practically infinite. Thus, diffusion-limited escape is neglected.

### Appendix C

#### Detectability of Spectral Features in $H_2$ -dominated Atmospheres

Here we discuss the locations and detectability of key spectral features in  $H_2$ -dominated atmospheres based on Figures 5 and 6. The most prominent feature in our model spectra is the  $H_2$ - $H_2$  CIA extending from  $\sim 6$  to  $20 \mu\text{m}$ . The Rayleigh scattering slope at  $\lesssim 1 \mu\text{m}$  is also dominated by  $H_2$  opacity, except in the 4000 K high outgassing case, where  $CH_4$  becomes pervasive in the atmosphere with a mixing ratio of 0.73.  $CH_4$  features at 1.7, 2.3, 3.4, and  $7.5 \mu\text{m}$  are strong in most scenarios.  $CO_2$  features are strong in the high outgassing models, with the  $4.2 \mu\text{m}$  feature being the most prominent because the  $15 \mu\text{m}$  feature is partially obscured by the broad  $H_2$ - $H_2$  CIA wing.  $H_2O$  features at 2.6 and  $6.4 \mu\text{m}$  are present in some models, especially in the 6000 K WD models where the  $CH_4$  feature at  $7.5 \mu\text{m}$  is relatively weak and does not completely overlap with the  $6.4 \mu\text{m}$  water feature. CO shows a strong feature at  $4.7 \mu\text{m}$ , which has comparable strength as the  $4.2 \mu\text{m}$   $CO_2$  feature and is not obscured by any overlapping stronger features. The potential of detecting CO in a large amount (the mixing ratios of CO range from  $8.0 \times 10^{-5}$  to  $3.7 \times 10^{-4}$  in the high outgassing models) in an  $H_2$ -dominated atmosphere is noteworthy, because CO is the best-studied species under the context of photochemical runaway (Schwieterman et al. 2019; Ranjan et al. 2022).

### Appendix D

#### Additional Results for $N_2$ - and $CO_2$ -dominated Atmospheres

##### D.1. Inferring Outgassing Activities of Planets with High MMW Atmospheres

As demonstrated in Section 3.3, high and low outgassing rates can be differentiated on rocky WD planets with  $H_2$  atmospheres, although inferring tectonic activities of rocky exoplanets from outgassing rates is limited by many uncertainties. Here, we focus on weakly and highly oxidizing atmospheres dominated by  $N_2$  or  $CO_2$  and quantitatively discuss the ability of JWST to distinguish between high and low outgassing scenarios for the  $N_2$ - and  $CO_2$ -dominated models.

Transmission spectra can differentiate between our high and low outgassing scenarios assuming  $N_2$  or  $CO_2$  atmospheres, albeit more telescope time is required due to the smaller extent of high MMW atmospheres. We compare simulated transmission spectra for our high and low outgassing scenarios in Figure 7 and show molecular contributions to the overall spectra in Figure 8 for  $N_2$ -dominated atmospheres. We show the same information for  $CO_2$ -dominated atmospheres in Figures 9 and 10. We model an array of campaign sizes with NIRSpec Prism, including 1, 5, 10, and 25 transits, and choose to show the 25-transit program. This is because programs with 10 or fewer transits have low S/N due to the small scale height of  $N_2$  and  $CO_2$  atmospheres.

For the  $N_2$ -dominated models,  $CH_4$  features at 1.7, 2.3, and  $3.4 \mu\text{m}$  are the keys to distinguishing between the high and low outgassing scenarios (Figure 7). The  $CO_2$  feature at  $4.2 \mu\text{m}$  also differs significantly between the two scenarios but is a less effective indicator due to lower S/N. For the 6000 K WD models,  $CH_4$  features differ by  $\sim 2.5\sigma$  between high and low outgassing scenarios. The  $CH_4$  mixing ratio rapidly increases when outgassing rates are high as effective temperature of the host WD decreases, due to the photochemical runaway mechanism discussed in Section 3.4. Therefore, high and low outgassing scenarios can be differentiated with larger significance for the 5000 K and 4000 K WD models.

For the  $CO_2$ -dominated models, high and low outgassing scenarios are not distinguishable with 25 NIRSpec Prism transits for the 6000 K and 5000 K WD models (Figure 9). In an oxidizing environment dominated by  $CO_2$ ,  $CH_4$  cannot efficiently accumulate even if the emission flux increases by a factor of 1000, explaining the lack of difference between the

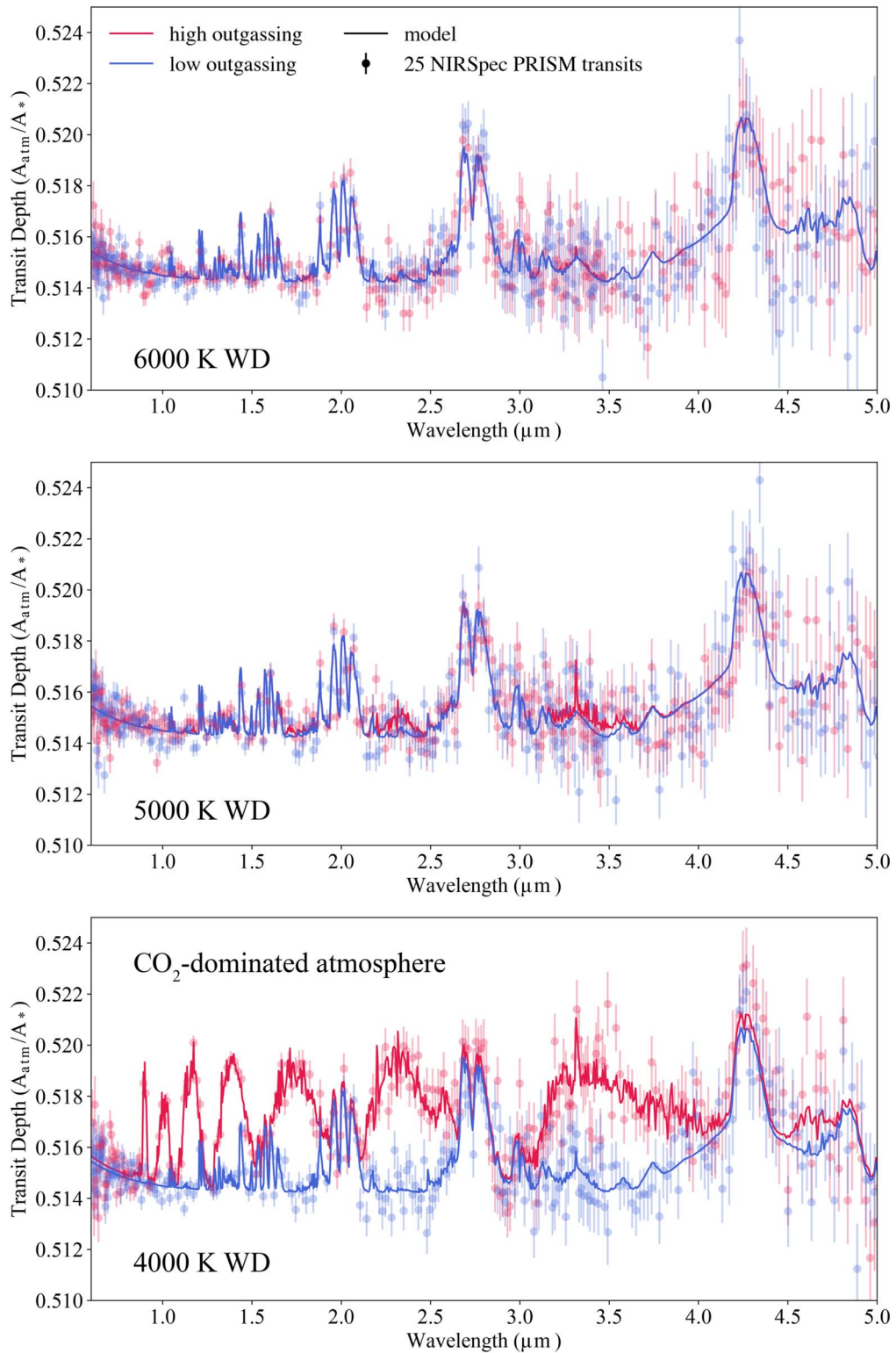


**Figure 9.** Transmission spectra models and simulated JWST transit observations for  $\text{CO}_2$ -dominated atmospheres, assuming a  $1 R_{\oplus}$  planet transiting WD 1856+534. We compare high outgassing rate models (red solid lines) with low outgassing rate models (blue solid lines) and show simulated JWST data points with their  $1\sigma$  error bars. We assume 25 NIRSpec Prism transits for the  $\text{CO}_2$ -dominated atmospheric models.  $\text{CO}_2$  features are detectable with 25 transits for all models, but distinguishing between high and low outgassing scenarios is only achievable for the 4000 K WD model, because  $\text{CH}_4$  only builds up to detectable levels in the 4000 K WD high outgassing scenario.

two scenarios. For the 4000 K WD models, however,  $\text{CH}_4$  provides an opportunity to distinguish between high and low outgassing rates, likely because emission of  $\text{CH}_4$  passes the low runaway threshold on a planet with extremely low UV

radiation. Using the  $\text{CH}_4$  features between 0.9 and 2.5  $\mu\text{m}$  as indicators, we may differentiate between the two outgassing scenarios at  $\sim 10\sigma$  significance with 25 transits, and at  $\sim 5\sigma$  with 10 transits.

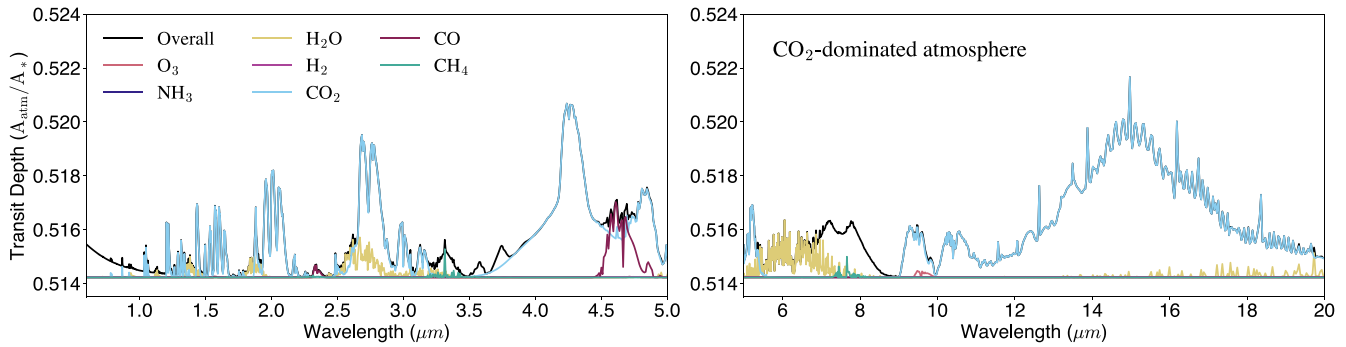


**Figure 10.** Molecular contributions to the overall model transmission spectra for  $\text{CO}_2$ -dominated atmospheres.

### D.2. Testing Photochemical Runaway in Oxidizing Atmospheres

Redox state impacts photochemical runaway (e.g., Ranjan et al. 2022). The main sink of  $\text{CH}_4$  is hydroxyl (OH) radicals, which is typically produced by  $\text{O}(^1\text{D})$  reacting with water. More oxidizing environments naturally lead to higher production of OH radicals, making the photochemical sink of  $\text{CH}_4$  harder to saturate. Indeed, the mixing ratio of  $\text{CH}_4$  is generally much lower in  $\text{N}_2$ - and  $\text{CO}_2$ -dominated models, compared to  $\text{H}_2$ -dominated models with the same outgassing rate and WD host (Table 2).

Nevertheless,  $\text{CH}_4$  runaway can occur in weakly oxidizing and oxidizing atmospheres, as evidenced by strong  $\text{CH}_4$  features in the 4000 K WD models for both atmospheric redox states (Figures 7 and 9). As a result of photochemical runaway,  $\text{CH}_4$  is easily detectable by JWST on rocky exoplanets transiting cool WDs. Here we quantitatively discuss  $\text{CH}_4$  detectability by NIRSpec Prism in our various models.

Detecting  $\text{CH}_4$  is more challenging in  $\text{N}_2$ -dominated atmospheres compared to  $\text{H}_2$ -dominated atmospheres but is still achievable within a small JWST program for the high outgassing scenarios. For the 4000 K WD model, which has the highest  $\text{CH}_4$  mixing ratios due to low UV radiation, five NIRSpec Prism transits can detect  $\text{CH}_4$  features at  $\sim 3\sigma$ – $4\sigma$ . For the  $\text{N}_2$  5000 K WD and  $\text{N}_2$  6000 K WD high outgassing models, detecting  $\text{CH}_4$  is more complicated— $\text{CH}_4$  features at  $< 2 \mu\text{m}$  partially or totally overlap with  $\text{H}_2\text{O}$  features with similar strength, while  $\text{CH}_4$  features at  $> 2 \mu\text{m}$  suffer from higher noise levels. Therefore, confidently detecting  $\text{CH}_4$  in  $\text{N}_2$ -dominated atmospheres with high outgassing rates based on the 1.7 and 2.3  $\mu\text{m}$  features requires 25 transits. For all of the low outgassing scenarios,  $\text{CH}_4$  is not detectable.

For the  $\text{CO}_2$ -dominated models,  $\text{CH}_4$  only reaches detectable levels via photochemical runaway in the 4000 K high outgassing scenario. In this case, five NIRSpec Prism transits can detect  $\text{CH}_4$  at  $\sim 3\sigma$ – $4\sigma$ , and 10 transits can achieve a conclusive  $\sim 5\sigma$  detection.

### D.3. Detectability of Spectral Features in $\text{N}_2$ - and $\text{CO}_2$ -dominated Atmospheres

Here we summarize the locations and detectability of key spectral features in  $\text{N}_2$ - and  $\text{CO}_2$ -dominated atmospheres based on simulated transmission spectra and JWST observations (Figure 7 for  $\text{N}_2$  atmospheres and Figure 9 for  $\text{CO}_2$  atmospheres). We also show the molecular contributions to the overall spectra (Figure 8 for  $\text{N}_2$  atmospheres and Figure 10 for  $\text{CO}_2$  atmospheres). Note that in Figure 5 we show JWST

observations with one NIRSpec Prism transit for the  $\text{H}_2$  models, but for  $\text{N}_2$ - and  $\text{CO}_2$ -dominated models, we show 25 transits, because high MMW  $\text{N}_2$  and  $\text{CO}_2$  atmospheres have lower atmospheric scale heights. Also note that we assume the stellar parameters of WD 1856+534 (Vanderburg et al. 2020). A brighter or more close-by host can increase S/N and hence detectability of spectral features.

In  $\text{N}_2$ -dominated atmospheric models,  $\text{H}_2\text{O}$  has strong features in all scenarios. The strongest water features are located at 2.6 and 6.4  $\mu\text{m}$ , with a few weaker features located at approximately 1.0, 1.2, 1.3, and 1.9  $\mu\text{m}$ , as well as the broad continuum from about 10 to 20  $\mu\text{m}$ . Water features at 1.0–2.6  $\mu\text{m}$  coincide with a bandpass in which noise levels are low and are likely detectable by NIRSpec Prism.  $\text{CO}_2$  features at 4.2 and 15  $\mu\text{m}$  are present but weaker than water features in the reduced outgassing models, but are predominant in the high outgassing models, where  $\text{CO}_2$  outgassing rates are 1000 times higher than in the reduced outgassing models. In the high outgassing models,  $\text{CH}_4$  also shows strong features at 3.4 and 7.5  $\mu\text{m}$ , as well as several weaker features in the visible wavelength range. As discussed in Appendix D.2, these  $\text{CH}_4$  features are detectable by NIRSpec Prism at high significance and can potentially differentiate between the high and low outgassing scenarios. In addition,  $\text{N}_2$ – $\text{N}_2$  has a CIA feature at 4.3  $\mu\text{m}$ , which overlaps with the 4.2  $\mu\text{m}$   $\text{CO}_2$  feature. In the reduced outgassing models, the  $\text{N}_2$ – $\text{N}_2$  CIA and the  $\text{CO}_2$  feature have similar strength and may lead to detection degeneracy.

In a  $\text{CO}_2$ -dominated atmosphere (90%  $\text{CO}_2$ ),  $\text{CO}_2$  features unsurprisingly dominate the transmission spectra. The strongest  $\text{CO}_2$  feature is at 15  $\mu\text{m}$ , with broad wings extending to about 11 and 20  $\mu\text{m}$  on each side. The second strongest  $\text{CO}_2$  feature is located at 4.2  $\mu\text{m}$  and is likely the most easily detectable feature for NIRSpec Prism. In addition,  $\text{CO}_2$  has a few weaker features at 1.4, 1.6, 1.9, 2.1, 2.8, 3.0, 4.8, 5.2, and 10.3  $\mu\text{m}$ . Other than single-molecule absorption features, a  $\text{CO}_2$ – $\text{CO}_2$  CIA feature is also present at about 7.5  $\mu\text{m}$ . CO has a feature at about 4.7  $\mu\text{m}$  but is obscured by the stronger  $\text{CO}_2$  feature at 4.8  $\mu\text{m}$ .  $\text{H}_2\text{O}$  has a broad feature at 6.4  $\mu\text{m}$ , which is the strongest feature of water and does not overlap with any other features.  $\text{H}_2\text{O}$  also has a continuum from about 10 to 20  $\mu\text{m}$ , several weak features in visible wavelengths, and a strong feature at 2.6  $\mu\text{m}$ , but all of these features are obscured by nearby  $\text{CO}_2$  features.  $\text{CH}_4$  has two broad features at 3.4 and 7.5  $\mu\text{m}$ , as well as several features in the visible and near-IR wavelengths spanning from 0.9 to 2.5  $\mu\text{m}$ .  $\text{CH}_4$  features are only strong enough to be detectable in the 5000 K and 4000 K high outgassing cases. Especially in the 4000 K high outgassing

scenario, CH<sub>4</sub> features have comparable strengths to the strongest CO<sub>2</sub> features and dominate the visible to near-IR wavelength range probed by NIRSPEC Prism.

### ORCID iDs

Zifan Lin  <https://orcid.org/0000-0003-0525-9647>  
 Sukrit Ranjan  <https://orcid.org/0000-0002-5147-9053>  
 Thea Kozakis  <https://orcid.org/0000-0002-3868-2129>  
 Lisa Kaltenegger  <https://orcid.org/0000-0002-0436-1802>

### References

- Agol, E. 2011, *ApJL*, 731, L31
- Airapetian, V. S., Gloer, A., Khazanov, G. V., et al. 2017, *ApJL*, 836, L3
- Arney, G., Domagal-Goldman, S. D., Meadows, V. S., et al. 2016, *AsBio*, 16, 873
- Arney, G., Domagal-Goldman, S. D., & Meadows, V. S. 2018, *AsBio*, 18, 311
- Arney, G. N., Meadows, V. S., Domagal-Goldman, S. D., et al. 2017, *ApJ*, 836, 49
- Batalha, N. E., Mandell, A., Pontoppidan, K., et al. 2017, *PASP*, 129, 064501
- Bear, E., & Soker, N. 2015, *MNRAS*, 450, 4233
- Bergeron, P., Leggett, S. K., & Ruiz, M. T. 2001, *ApJS*, 133, 413
- B  tr  mieux, Y., & Kaltenegger, L. 2014, *ApJ*, 791, 7
- Blackman, J. W., Beaulieu, J. P., Bennett, D. P., et al. 2021, *Natur*, 598, 272
- Catling, D. C., & Kasting, J. F. 2017, *Atmospheric Evolution on Inhabited and Lifeless Worlds* (Cambridge: Cambridge Univ. Press), doi:10.1017/9781139020558
- Chen, H., Wolf, E. T., Zhan, Z., & Horton, D. E. 2019, *ApJ*, 886, 16
- Cort  s, J., & Kipping, D. 2019, *MNRAS*, 488, 1695
- Coutu, S., Dufour, P., Bergeron, P., et al. 2019, *ApJ*, 885, 74
- Davies, J. H., & Davies, D. R. 2010, *SoIe*, 1, 5
- de Pater, I., & Lissauer, J. J. 2001, *Planetary Sciences* (Cambridge: Cambridge Univ. Press)
- Dong, C., Huang, Z., Lingam, M., et al. 2017, *ApJL*, 847, L4
- Dorn, C., Noack, L., & Rozel, A. B. 2018, *A&A*, 614, A18
- Doyle, A. E., Young, E. D., Klein, B., Zuckerman, B., & Schlichting, H. E. 2019, *Sci*, 366, 356
- Elkins-Tanton, L. T., & Seager, S. 2008, *ApJ*, 685, 1237
- Farihi, J., Koester, D., Zuckerman, B., et al. 2016, *MNRAS*, 463, 3186
- Fischer, T. P. 2008, *GeocJ*, 42, 21
- Foley, B. J., & Smye, A. J. 2018, *AsBio*, 18, 873
- Fontaine, G., & Brassard, P. 2008, *PASP*, 120, 1043
- Fontaine, G., Brassard, P., & Bergeron, P. 2001, *PASP*, 113, 409
- Fossati, L., Bagnulo, S., Haswell, C. A., et al. 2012, *ApJL*, 757, L15
- Gaillard, F., & Scaillet, B. 2014, *E&PSL*, 403, 307
- Gillmann, C., & Tackley, P. 2014, *JGRE*, 119, 1189
- Grimm, S. L., & Heng, K. 2015, *ApJ*, 808, 182
- Guillot, T. 2010, *A&A*, 520, A27
- Harman, C. E., Kopparapu, R., Stefansson, K., et al. 2021, arXiv:2109.10838
- Holland, H. D. 1984, *The Chemical Evolution of the Atmosphere and Oceans* (Princeton, NJ: Princeton Univ. Press)
- Hu, R., Seager, S., & Bains, W. 2012, *ApJ*, 761, 166
- Huang, J., Seager, S., Petkowski, J. J., Ranjan, S., & Zhan, Z. 2021, arXiv:2107.12424
- Hunten, D. M. 1973, *JAtS*, 30, 1481
- James, T., & Hu, R. 2018, *ApJ*, 867, 17
- Kaltenegger, L., MacDonald, R. J., Kozakis, T., et al. 2020, *ApJL*, 901, L1
- Kasting, J. F., & Catling, D. 2003, *ARA&A*, 41, 429
- Kasting, J. F., Whitmire, D. P., & Reynolds, R. T. 1993, *Icar*, 101, 108
- Keller-Rudek, H., Moortgat, G. K., Sander, R., & S  rensen, R. 2013, *ESSD*, 5, 365
- Kepler, S. O., Pelisoli, I., Koester, D., et al. 2016, *MNRAS*, 455, 3413
- Kite, E. S., Fegley, B., Jr., Schaefer, L., & Ford, E. B. 2020, *ApJ*, 891, 111
- Kite, E. S., Fegley, Bruce, Jr., Schaefer, L., & Ford, E. B. 2019, *ApJL*, 887, L33
- Komacek, T. D., Fauchez, T. J., Wolf, E. T., & Abbot, D. S. 2020, *ApJL*, 888, L20
- Kozakis, T., & Kaltenegger, L. 2019, *ApJ*, 875, 99
- Kozakis, T., Kaltenegger, L., & Hoard, D. W. 2018, *ApJ*, 862, 69
- Kozakis, T., Lin, Z., & Kaltenegger, L. 2020, *ApJL*, 894, L6
- Kulikov, Y. N., Lammer, H., Lichtenegger, H. I. M., et al. 2007, *SSRv*, 129, 207
- Lederberg, J. 1965, *Natur*, 207, 9
- Lenardic, A., Jellinek, A. M., Foley, B., O'Neill, C., & Moore, W. B. 2016, *JGRE*, 121, 1831
- Lin, Z., MacDonald, R. J., Kaltenegger, L., & Wilson, D. J. 2021, *MNRAS*, 505, 3562
- Loeb, A., & Maoz, D. 2013, *MNRAS*, 432, L11
- Lopez, E. D., & Fortney, J. J. 2013, *ApJ*, 776, 2
- Luger, R., & Barnes, R. 2015, *AsBio*, 15, 119
- Malamud, U., & Perets, H. B. 2017, *ApJ*, 849, 8
- Marley, M. S., Ackerman, A. S., Cuzzi, J. N., & Kitzmann, D. 2013, in *Clouds and Hazes in Exoplanet Atmospheres*, ed. S. J. Mackwell (Tucson, AZ: Univ. Arizona Press), 367
- Molli  re, P., Wardenier, J. P., van Boekel, R., et al. 2019, *A&A*, 627, A67
- Ortenzi, G., Noack, L., Sohl, F., et al. 2020, *NatSR*, 10, 10907
- Owen, J. E., Shaikhislamov, I. F., Lammer, H., Fossati, L., & Khodachenko, M. L. 2020, *SSRv*, 216, 129
- Owen, J. E., & Wu, Y. 2013, *ApJ*, 775, 105
- Owen, J. E., & Wu, Y. 2017, *ApJ*, 847, 29
- Perryman, M., Hartman, J., Bakos, G. A., & Lindegren, L. 2014, *ApJ*, 797, 14
- Ramirez, R. M., & Kaltenegger, L. 2016, *ApJ*, 823, 6
- Ramirez, R. M., Kopparapu, R., Zuger, M. E., et al. 2014, *NatGe*, 7, 59
- Ranjan, S., Schwietzman, E. W., Harman, C., et al. 2020, *ApJ*, 896, 148
- Ranjan, S., Seager, S., Zhan, Z., et al. 2022, arXiv:2201.08359
- Ranjan, S., Todd, Z. R., Sutherland, J. D., & Sasselov, D. D. 2018, *AsBio*, 18, 1023
- Rey, P. F., Coltice, N., & Flament, N. 2014, *Natur*, 513, 405
- Robinson, T. D., Fortney, J. J., & Hubbard, W. B. 2017, *ApJ*, 850, 128
- Roble, R. G., Ridley, E. C., & Dickinson, R. E. 1987, *JGR*, 92, 8745
- Saumon, D., Holberg, J. B., & Kowalski, P. M. 2014, *ApJ*, 790, 50
- Scaillet, B., & Gaillard, F. 2011, *Natur*, 480, 48
- Schaefer, L., & Fegley, B. 2010, *Icar*, 208, 438
- Schreiber, M. R., G  nsicke, B. T., Toloza, O., Hernandez, M.-S., & Lagos, F. 2019, *ApJL*, 887, L4
- Schr  der, K. P., & Smith, R. C. 2008, *MNRAS*, 386, 155
- Schwietzman, E. W., Reinhard, C. T., Olson, S. L., et al. 2019, *ApJ*, 874, 9
- Seager, S., Bains, W., & Hu, R. 2013, *ApJ*, 777, 95
- Segura, A., Kasting, J. F., Meadows, V., et al. 2005, *AsBio*, 5, 706
- Sengupta, S. 2016, *JApA*, 37, 11
- Sousa-Silva, C., Seager, S., Ranjan, S., et al. 2020, *AsBio*, 20, 235
- Stephan, A. P., Naoz, S., & Zuckerman, B. 2017, *ApJL*, 844, L16
- Suissa, G., Mandell, A. M., Wolf, E. T., et al. 2020, *ApJ*, 891, 58
- Tian, F., Kasting, J. F., Liu, H.-L., & Roble, R. G. 2008, *JGR*, 113, E05008
- Trail, D., Watson, E. B., & Tailby, N. D. 2011, *Natur*, 480, 79
- van Lieshout, R., Kral, Q., Charnoz, S., Wyatt, M. C., & Shannon, A. 2018, *MNRAS*, 480, 2784
- van Sluijs, L., & Van Eylen, V. 2018, *MNRAS*, 474, 4603
- Vanderburg, A., Rappaport, S. A., Xu, S., et al. 2020, *Natur*, 585, 363
- Veras, D., & G  nsicke, B. T. 2015, *MNRAS*, 447, 1049
- Veras, D., Shannon, A., & G  nsicke, B. T. 2014, *MNRAS*, 445, 4175
- Watson, A. J., Donahue, T. M., & Walker, J. C. 1981, *Icar*, 48, 150
- Weller, M., Lenardic, A., & O'Neill, C. 2015, *E&PSL*, 420, 85
- Wood, B. J., Walter, M. J., & Wade, J. 2006, *Natur*, 441, 825
- Yang, J., Bou  , G., Fabrycky, D. C., & Abbot, D. S. 2014, *ApJL*, 787, L2
- Zhan, Z., Seager, S., Petkowski, J. J., et al. 2021, *AsBio*, 21, 765